Experimental and CFD Study of KCS Hull-Propeller-Rudder Interaction for Self-Propulsion and Port and Starboard Turning Circles

Professor Frederick Stern
The University of Iowa, IIHR, Iowa City, IA USA
Plenary lecture 4th CMHL Symposium online January 14, 2021

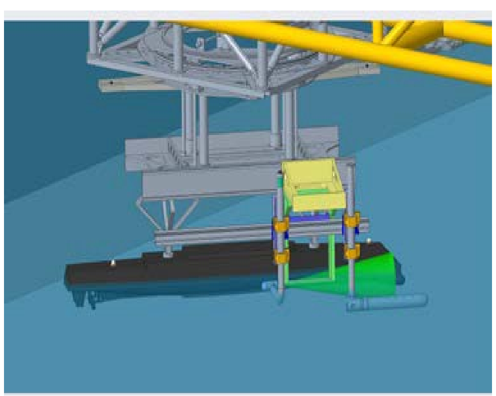

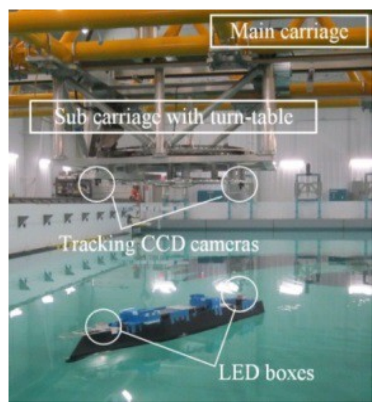

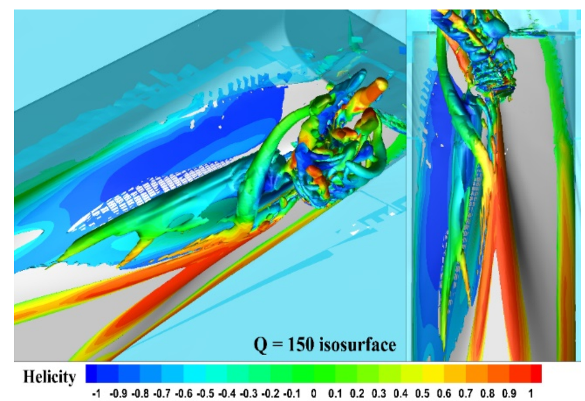

Manuscript submitted Journal Applied Ocean Research, January 2021; Co-authors Yugo Sanada, Sungtek Park, Dong Hwan Kim, Zhaoyuan Wang, Hironori Yasukawa and Frederick Stern

Outline

1. Background

a. Yugo Sanada, Dong-Hwan Kim, Hamid Sadat-Hosseini, Frederick Stern, Md Alfaz Hossain, Ping-Chen Wu, Yasuyuki Toda, Janne Otzen, Claus Simonsen, Moustafa Abdel-Maksoud, Martin Scharf, Gregory Grigoropoulos," **Assessment of Experimental and CFD Capability for KCS Added Power in Head and Oblique Waves," 33rd Symposium on Naval Hydrodynamics**, week of 18 October 2020 using a virtual format.

b. Yugo Sanada, Sungtek Park, Frederick Stern, Frans Quadvlieg, Milanov Evgeni, Wentao Wang, Hironori Yasukawa, Dongjin Kim, Yasuyuki Toda, Matteo Diez, "**Assessment of Free-Running Model Tests for KCS Maneuvering in Calm Water and Waves & Comparison with CFD," SIMMAN 2021 and submission** Journal Applied Ocean Research.

2. Objectives

Physics and scaling Correlations for Maneuvering in Calm Water and Waves

3. Approach (Fr=0.157)

a. Propeller load scaling for maneuvering

b. MMG Rudder Model and Beaufoy's Formula

c. Experimental/MMG Assessment of KCS Port and Starboard Turning Circles

d. CFD Assessment and Validation of KCS Port and Starboard Turning Circles

e. CFD Assessment of Hull-Propeller-Rudder Interaction

4. Overall Conclusions and Prognosis Maneuvering In waves

Appendix: Results for Fr=0.026

Acknowledgements: The research at IIHR was supported by the Office of Naval Research grants N00014-17-1-2083 and N00014-17-1-2084 under administration Drs. Thomas Fu, Woei-Min Lin and Ki-Han Kim sponsored this research. The simulations were performed using DoD, Navy DSRC HPCMP resources including 18 Pathfinder program allocations. The SIMMAN 2020 Organizing Committee and Drs. Thad Michael, Serge Toxopeous and Matteo Diez provided helpful discussions.

Introduction

- The physics of ship maneuvering are poorly understood, and prediction capability is lacking in comparison to resistance and propulsion and seakeeping, as evidenced by the ITTC proceedings and most recent CFD (Hino et al., 2020) and SIMMAN (Quadvlieg et al., 2021) workshops, although progress has been made as evidenced comparison most recent and previous SIMMAN (Simonsen et al., 2017) workshops. Similarly, the measurement capability is reduced since requires free running models in maneuvering basins, which is less mature than captive model testing as evidenced by recent facility bias/scale effects studies for KCS added power (Sanada et al., 2020) vs. maneuvering in calm water and waves (Sanada et al., 2021).

- Herein, the focus is on physical understanding of hull-propeller-rudder interaction for calm water port vs. starboard turning circles for the KRISO container ship (KCS), which is a benchmark geometry used for both CFD and SIMMAN workshops. Although KCS is a single screw ship, the results will be clearly shown to also help explain the physics for twin screw ships and zig-zag maneuvers albeit without transient effects, i.e., for larger rudder deflections. Several previous studies have noted the differences for port vs. starboard maneuvering such as Schot and Eggars (2019), Kuiper et al. (2002) and Schulten et al. (2004) but have not provided a satisfactory explanation.

- The overall objective is to provide physics and scaling correlations for ship maneuvering in calm water and waves with the present contribution being the focus as previously stated. The approach is using propeller load scaling and Maneuvering Modeling Group (MMG) rudder and 3DoF maneuvering modeling (Yasukawa and Yoshimura, 2015) to supplement experiments for CFD validation and analysis of the hull-propeller-rudder interaction to explicate the origin of the differences for port vs. starboard maneuvering.

Previous studies

- J. J. A. Schot and R. Eggers, "The Effect of Leeway Angle On The Propeller Performance," Wind Propulsion, 15th -16th October 2019, London, UK.

  It is observed that the general trend in the asymmetry in w_T at positive and negative leeway angles is well captured, this asymmetry is also reported in literature [3]. It is caused by the pre-swirl in the wake field in combination with the rotation direction of the propeller.

  [3] KOSE K., 'On a new mathematical model of maneuvering motions of a ship and its applications', International Shipbuilding Progress vol.29 no.336 pp. 205-220, 1982

- G. Kuiper, M. Grimm, B. McNeice, D. Noble, M.Krikke, "Propeller Inflow at Full Scale During a Manoeuvre," 24th Symposium on Naval Hydrodynamics Fukuoka, JAPAN, 8-13 July 2002

  It was found that the transverse velocities in the propeller plane were almost fully responsible for changes in power absorption in a turn. The mean axial velocity was about equal for the inner and the outer propeller in a turn. Unexpectedly the transverse velocities induced by a turn were small in the upper half of the propeller plane. The effects of the inflow measurements on the cavitation inception speed have also been estimated analytically.

- Lt P J M Schulten, S L Toxopeus, and D Stapersma, "Propeller - diesel engine interaction in a turn," 7 the International Naval Engineering Conference and Exhibition (INEC), London, UK, March 2004.

  This exhaust gas temperature can reach unexpected high values in a turn. Finally, in a twin-shaft configuration, the inner and outer propellers are loaded differently because of differences in wake. This results in difference in loading and exhaust gas temperature of the diesel engines.

Propeller load scaling for maneuvering

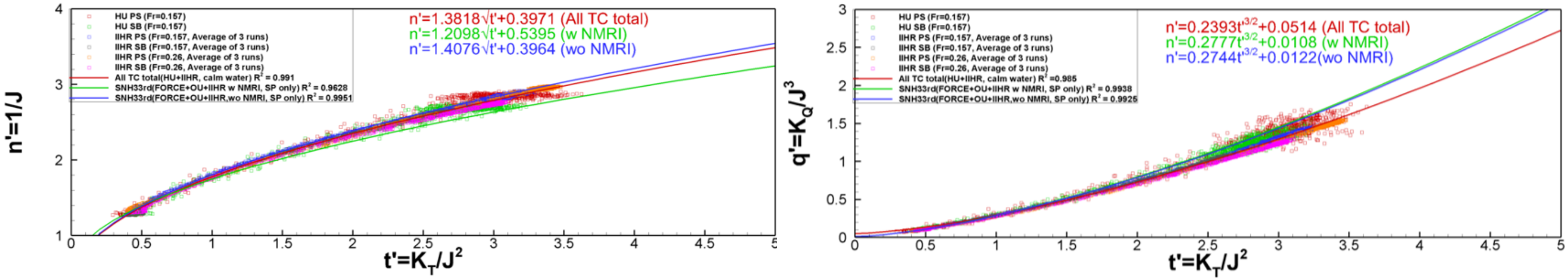

Figure 1. n' (left)and q'(right) vs. t' correlation for KCS maneuvering in calm water

- The usual propeller thrust K_T and torque K_Q scaling used for open water performance shows large scatter, whereas the Adachi and Sugai (1978) $q'(t')=K_Q/J^3$ and $n'(t')=t'/2pq'$ scaling where $t'=K_T/J^2$ shows good correlation for added power studies of facility bias/scale effects (Sanada et al., 2020). The reason is that the t' scaling depends on the hull size with D^2 replace by $\nabla^{2/3}$ where D is the propeller diameter and ∇ is the hull displacement volume. The Adachi and Sugai (1978) scaling are also used by ITTC 1978 ITTC Performance Prediction Method to predict speed-power-rpm relationship in waves, where the resistance and thrust identity method or direct powering method is applied (Yu et al. 2020).

- Figure 1 extends the q', n' and t' correlation for KCS maneuvering in calm water (also for waves, but results not shown), including comparisons with the previous added power studies. The results show that t' has a similar correlation as added power/course keeping (head and oblique waves), but much larger range and scatter. Different size models move up/down the t' correlation curve depending propeller loading during the turning circle (TC) and zigzag (ZZ) and both calm water and waves maneuvers (ZZ and waves results not shown). Model size scale effects need more study, as more complex than added power/course keeping. System based propeller models should use t' correlation vs. current propeller open water curve and J=U(1-w)/nD similar as CFD noninteractive axisymmetric body force model.

MMG Rudder Model and Beaufoy's Formula

Table 1. Steady state rudder normal force comparison of MMG rudder model and Beaufoy's formula with experiments and CFD

Facility	Fr	δ [deg]	Type	U (Steady) [m/s]	U_0 (Desired) [m/s]	U/U_0	F'_N (U(Steady))	F'_N (U_0(Desired)	F'_N (Beaufoy, U_0(Desired))	F_N (Measured) [N]	C_F $\left[\frac{F_N}{\frac{1}{2}\rho V^2 A_R}\right]$	F_N (Beaufoy, U_0(Desired)) [N]	F_N (MMG) [N]
HU (EFD)	0.157	35	PS	0.382	0.860	0.444	4.415	0.871	0.875	2.589	0.876	2.599	2.6
	0.157	-35	SB	0.410	0.860	0.477	4.325	-0.984	-0.875	2.922	0.988	2.599	2.9
MARIN(EFD)	0.26	35	PS	0.790	2.006	0.394	4.044	0.627	0.875	40	0.627	55.817	52.34
IIHR (CFD)	0.157	-35	SB	0.438	0.808	0.542	2.198	-0.646	-0.875	1.328	0.649	1.799	1.496
	0.157	35	PS	0.394	0.808	0.488				1.502	0.734		
	0.26	35	PS	0.658	1.338	0.492	3.071	0.743	0.875	4.188	0.746	4.934	4.507

Table 2. MMG model l'_R and γ_R coefficients

	MARIN	HU		IIHR	
	Port	Port	Starboard	Port	Starboard
l'_R	-0.9	-0.7739		-0.9	
γ_R	0.5	0.35	0.20	0.45	0.55

The MMG rudder model is as follows

$$X_R = -(1-t_R) F_N \sin\delta$$
$$Y_R = -(1+a_H) F_N \cos\delta$$
$$N_R = -(x_R + a_H x_H) F_N \cos\delta$$

The Beaufoy's formula is much simpler as follows:

$$\begin{cases} F_N = 58.8 g A_R U_r^{\,2} \sin\delta \\ U_r = 1.15U \quad \text{(Single screw, single rudder)} \end{cases}$$

- Both models follow a two-step procedure: (1) determine non-dimensional rudder normal force F_N; and (2) determine rudder forces and moment X_R, Y_R, N_R. Table 1 provides a steady state rudder normal force comparison of Beaufoy's formula and MMG rudder models with experiments and CFD. Both models are empirical and lacking enough physics. The MMG model is more complex with l'_R and γ_R coefficients that enable tuning. F_N was tuned using Hiroshima University (HU) experimental data, as provided in Table 2. Many issues including correct nondimensional form, i.e., using approach or maneuvering speed etc., which needs more study. As shown in Table 1 both models compare well with the experimental data for HU but not as well with the data from MARIN and with the CFD results; since, in these cases tuning was not done.

MMG Rudder Model and Beaufoy's Formula

Identification of hydrodynamic interaction coefficients between ship hull and rudder (t_R, a_H and x_H) in MMG model by CFD

$$X_R = -(1-t_R)F_N \sin\delta$$
$$Y_R = -(1+a_H)F_N \cos\delta$$
$$N_R = -(x_R + a_H x_H)F_N \cos\delta$$

a_H: Rudder force increase factor
t_R: Steering resistance deduction factor
x_H: Longitudinal coordinate of acting point of the additional lateral force
x_R: Longitudinal coordinate of rudder position (= -0.5L)

Estimation formula of hydrodynamic interaction coefficients (Kijima model)

$$\begin{cases} C_b = 0.6505 \\ t_R = 1-(0.28C_b + 0.55) \\ a_H = 2.32C_b^2 - 0.904C_b + 0.0276 \\ x_H/L = 9.64C_b^2 - 8.22C_b + 0.0077 \\ x_R/L = -0.5 \end{cases}$$

Table 3. Comparison between hydrodynamic interaction coefficients between Kijima model and CFD direct estimation

Variables	Kijima model	Direct estimation by CFD
t_R	0.2679	-0.0636
a_H	0.4213	-0.0312
x_H/L	-1.2602	-1.0160

- Table 3 compares the hydrodynamic interaction coefficients between the Kijima model and CFD direct estimation, which leads to the magnitude of the x-axis rudder generating force (X_R) is greater than the value obtained from the rudder normal force (F_N·sinδ) while the magnitude of the y-axis rudder generating force (Y_R) is less than F_N·cosδ.

Experimental/MMG Assessment of KCS Port and Starboard Turning Circles

- The recent facility bias/scale effects study for KCS maneuvering in calm water and waves (Sanada et al., 2021), included port and starboard 35° turning circles from six facilities for Fr=0.26 and from 3 facilities for Fr=0.157, as shown in Figure 2 along with results from CFDShip-Iowa. Sanada et al. (2021) and its references provide more details about the experimental methods, including feature engineering for identification for identification of the primary variables; however, herein the focus is specifically on the calm water port and starboard turning circle data. The MARIN and HU data was also used as test cases for the SIMMAN 2021 workshop.

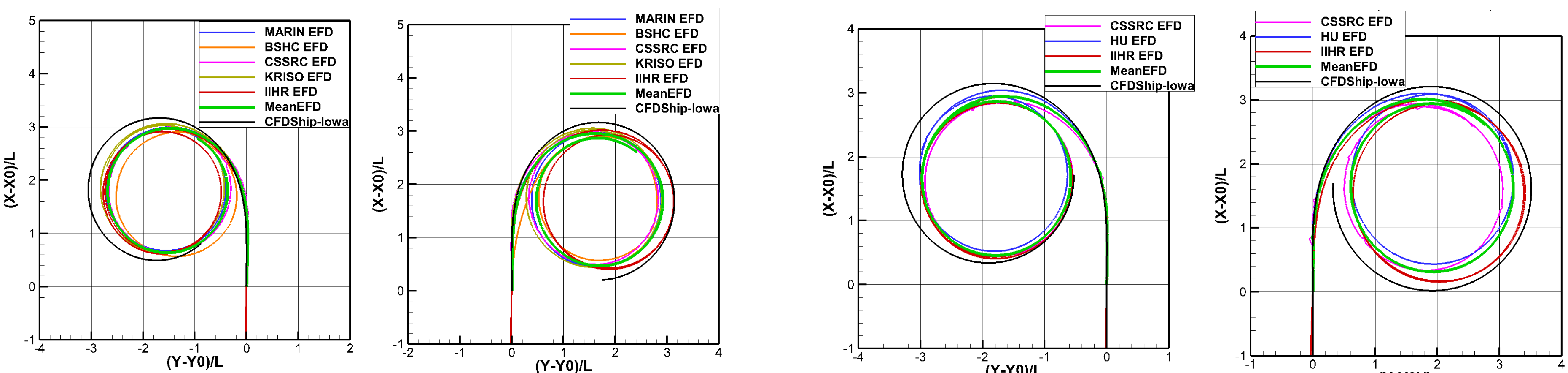

Port Side | Starboard Side | Port Side | Starboard Side

Fr #: 0.26 | **Fr #: 0.157**

Figure 2 (a). Trajectory of 35° Turning Circle in calm water

Experimental/MMG Assessment of KCS Port and Starboard Turning Circles

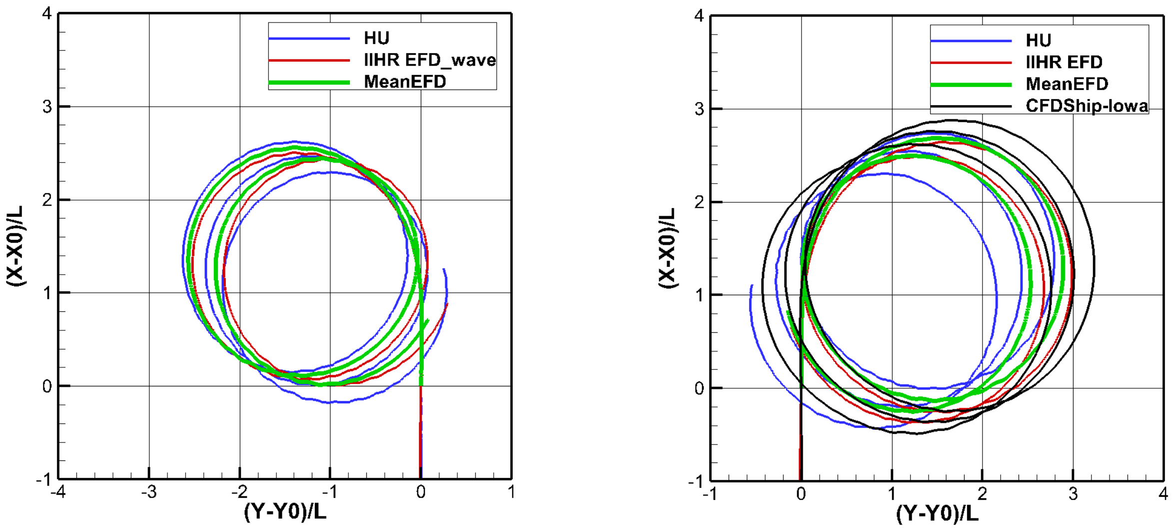

Figure 2 (b). Trajectory of 35º Turning Circle with Fr=0.157 in waves (Left: Port Side, Right: Starboard Side)

IIHR Port Turning in Waves

- The trends for Fr=0.26 were as follows: starboard mean (M) TD=AD=2.9L and R = 1.24L with SD = 5.9, 3.2 and 4.1%M; port mean TD=2.6L, AD =2.9L and R=1.17L with SD = 5.9, 3.2, and 2%M; port R is 6%M smaller than starboard; CFD predicts 9.5%M smaller for port than starboard; and port speed loss u=0.447U is larger than starboard u=0.465U. The results for Fr=.157 are similar, i.e.: starboard mean TD=3.2L, AD=2.9L and R = 1.3L with SD = 5.9, 3.2 and 4.1%M; port mean TD=AD =2.9L and R=1.2L with SD = 1.8, 3.3, and 1.1%M; port R is 8%M smaller than starboard; CFD predicts 12.7%M smaller for port than starboard; and port speed loss u=0.455U is larger than starboard u=0.488U.

Experimental/MMG Assessment of KCS Port and Starboard Turning Circles

- The IIHR wave basin experiments used a 2.7 m free running model with measurements of 6DoF and propeller revolutions, thrust and torque (n, T and Q). The HU experiments used a 3.2 m free running model with measurements of 6DoF, n, T, Q and rudder normal force F_N. The 3DoF MMG Model of Yasukawa and Yoshimura (2015) is as follows:

$$\dot{u}' = \frac{X'_H - R'_0 + X'_R + X'_P + \left(m' + m'_y\right)v'r'}{m' + m'_x} = \frac{\Delta X'}{m' + m'_x}$$

$$\dot{v}' = \frac{Y'_H + Y'_R - \left(m' + m'_x\right)u'r'}{m' + m'_y} = \frac{\Delta Y'}{m' + m'_y}$$

$$\dot{r}' = \frac{N'_H + N'_R}{I'_z + J'_z} = \frac{\Delta N'}{I'_z + J'_z}$$

- The terms in the 3DoF equations were evaluated using the IIHR experimental data supplemented with the MMG model for the hydrodynamic and rudder coefficients. Similarly, the terms in the 3DoF equations were evaluated using the HU experimental data supplemented with the MMG model for the hydrodynamic coefficients. For both facilities, the same resistance coefficient, hydrodynamic derivatives and added mass coefficients are used to evaluate R'_0, X'_H, Y'_H and N'_H (Hasnan and Yasukawa ,2020). X'_P is estimated by measured T. Added mass coefficients (m'_x, m'_y, J'_z) are estimated by Motora's empirical charts. The 3DoF force and moment balance was done for both Fr with similar results; however, since experimental data is also available from IIHR and HU for port and starboard 35^o turning circles in waves and the CFDShip-Iowa studies include additional simulations without the propeller and/or rudder for Fr=0.157 those results are the presented herein.

Experimental/MMG Assessment of KCS Port and Starboard Turning Circles

- It is important to recognize that the drift angle variation for turning circles is as follows:

✓ Drift Angle Variation for turning circles

$$v_o(t) = v_G(t) - LCG \cdot r_G(t)$$

$$\beta_O(t) = \mathrm{Tan}^{-1}\left(\frac{v_o(t)}{u(t)}\right)$$

$$\beta_x(x,t) = \beta_O(t) - x'r'$$

$$-\frac{1}{2} \le x' \le \frac{1}{2}, \left(FP : x = \frac{1}{2}, AP : x = -\frac{1}{2}, Midship : x = 0\right)$$

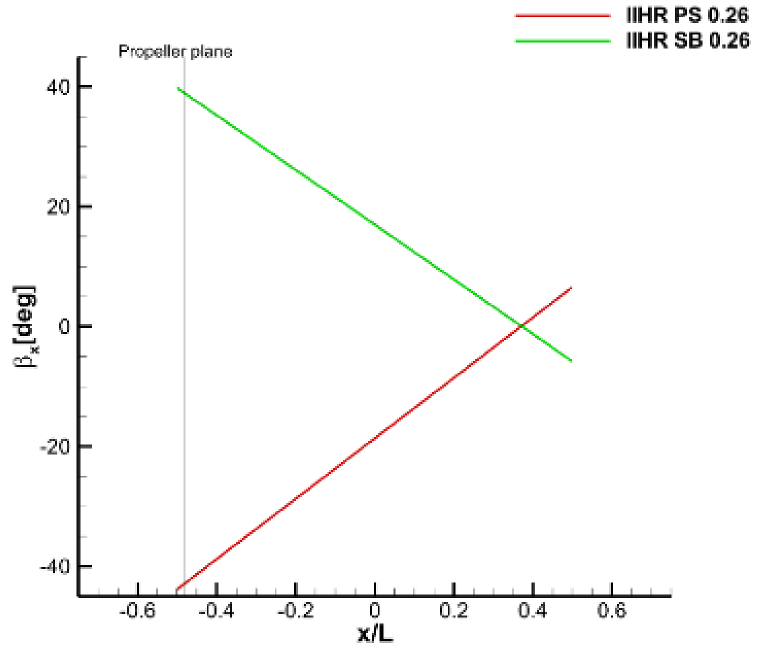

Figure 3. IIHR drift angle β(x) along the center line from AP to FP at Fr = 0.26

- The IIHR drift angle β(x) along the center line from AP to FP at Fr = 0.26 is shown in Figure 3. The drift angle varies for about 10° at the FP to 40° at the AP and is positive for starboard and negative for port.

Experimental/MMG Assessment of KCS Port and Starboard Turning Circles

KCS nondimensional force balance HU turning at Fr = 0.157

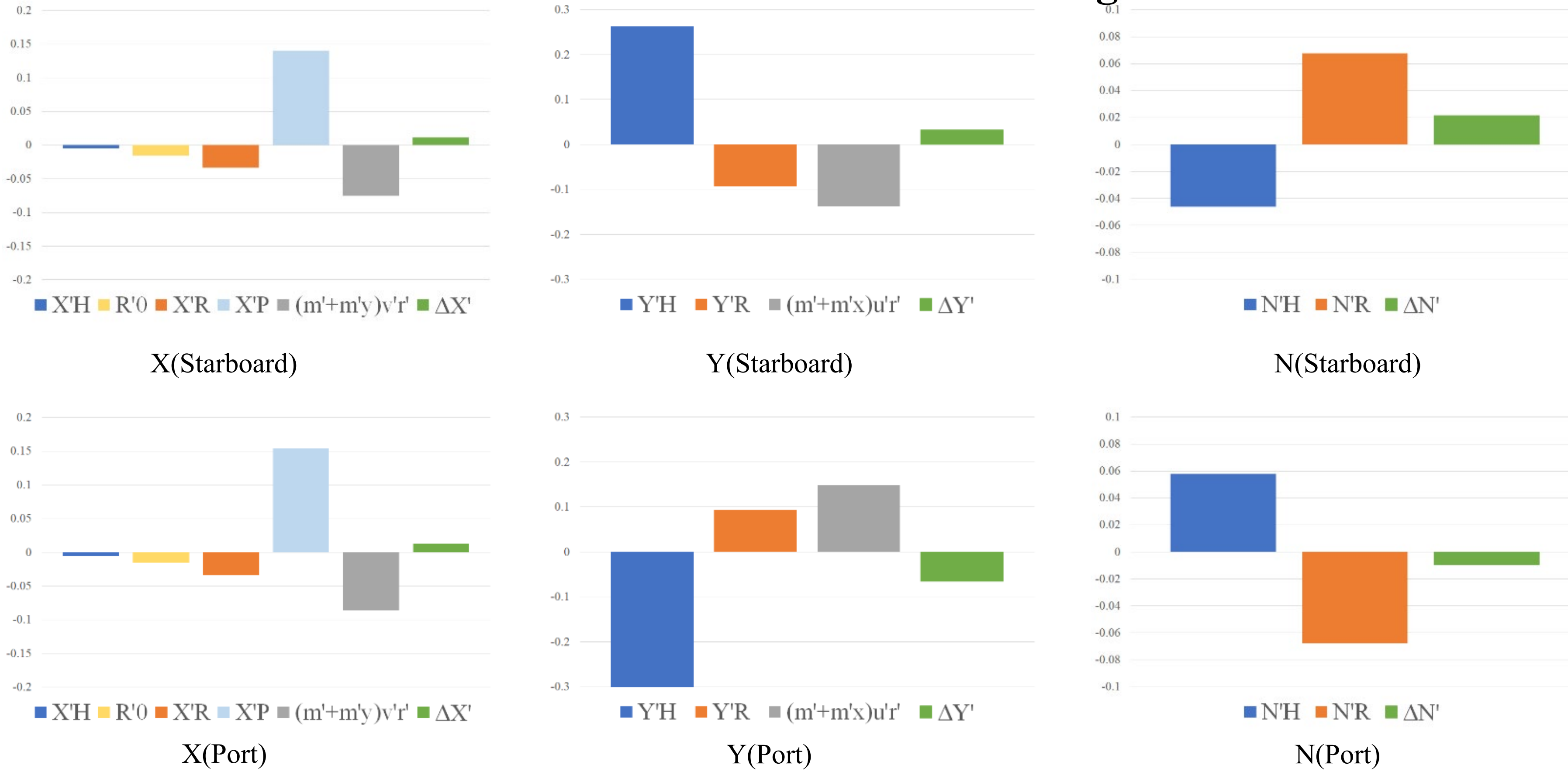

Figure 4. KCS nondimensional force and moment balance for HU turning at Fr = 0.157

- Figure 4 shows that the force and moment balance for HU has similar trends both port and starboard turning. The X_P is balanced mostly by inertia, but also X_R, R_0 and X_H. The Y_H is balanced mostly by inertia and, also Y_R. The N_H is balanced by N_R.

Experimental/MMG Assessment of KCS Port and Starboard Turning Circles

KCS nondimensional force balance IIHR turning at Fr = 0.157

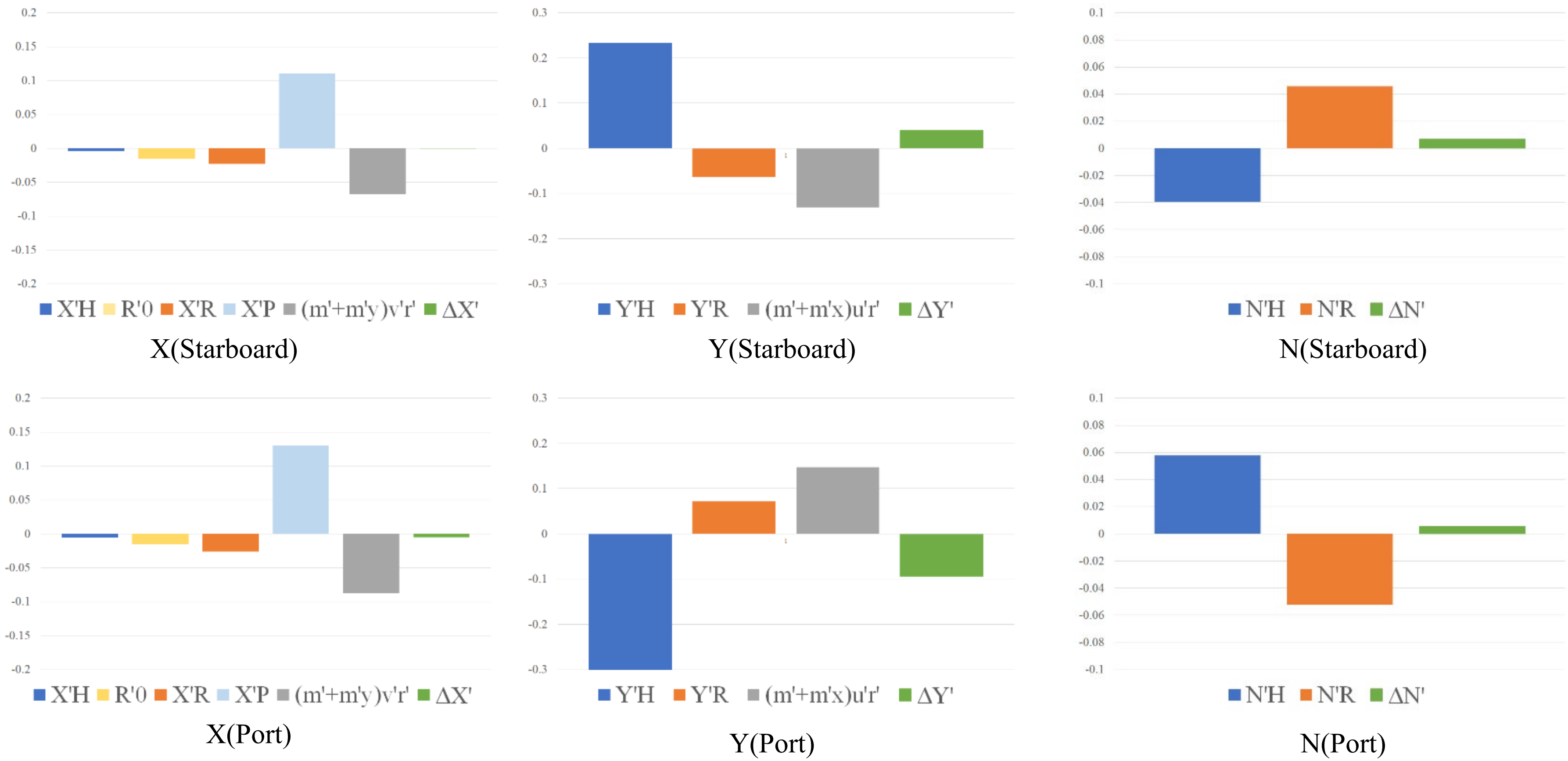

Figure 5. KCS nondimensional force and moment balance for IIHR turning at Fr = 0.157

- Figure 5 shows that the force and moment balance for IIHR has similar trends for both port and starboard turning as HU For both HU and IIHR the errors in the balances are reasonably small.

Experimental/MMG Assessment of KCS Port and Starboard Turning Circles

Nondimensional force and moment $\{|D_S|-|D_P|\}$ comparison between HU and IIHR at Fr=0.157

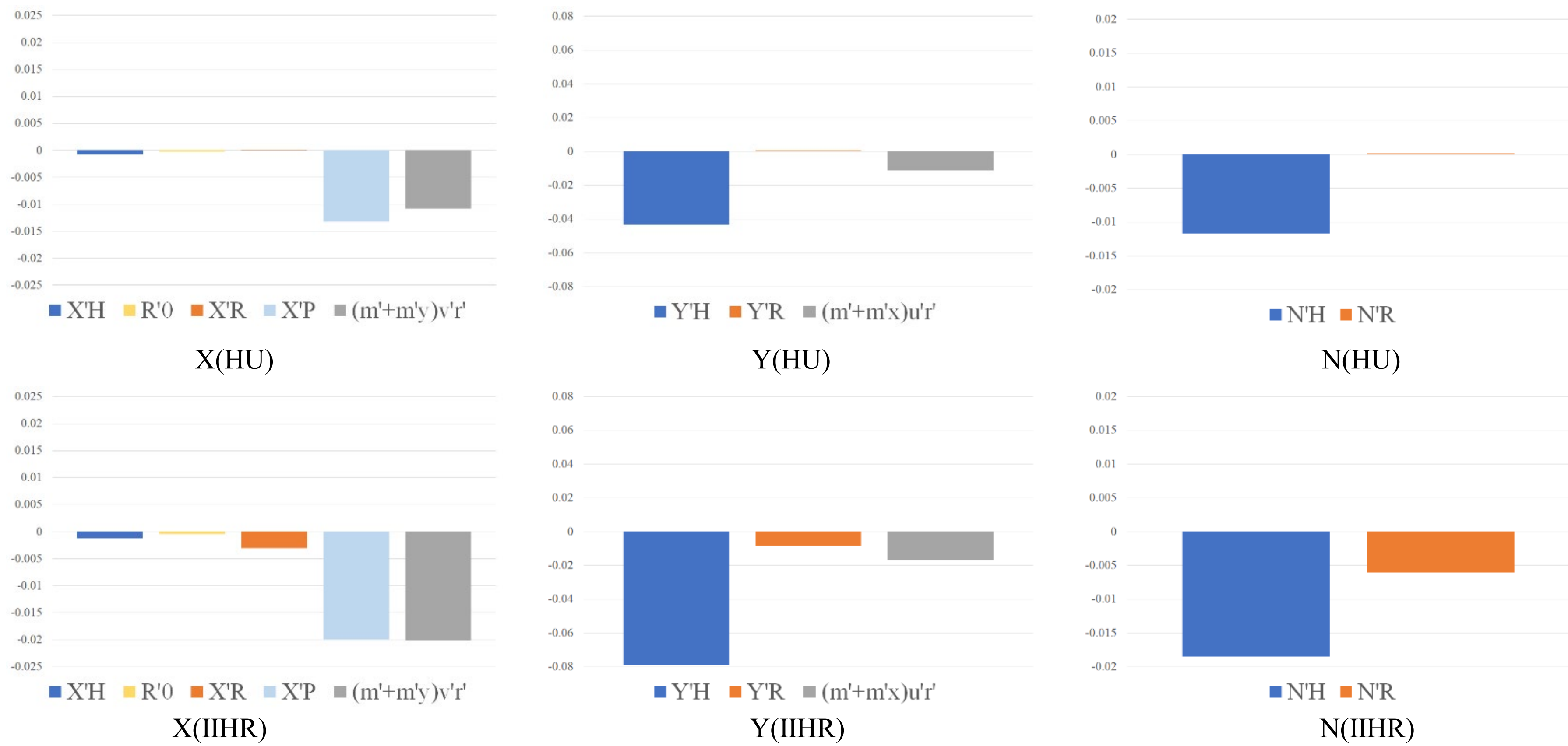

Figure 6. Nondimensional force and moment $\{|D_S|-|D_P|\}$ comparison between HU and IIHR at Fr=0.157

- Figure 6 shows the nondimensional force and moment ΔD=(starboard-port) comparison between HU and IIHR. All force and moment components have larger magnitudes for port vs. starboard turning.

CFD Assessment and Validation of KCS Port and Starboard Turning Circles

- Sanada et al. (2021) includes verification and validation assessment of CFDShip-Iowa results for both Fr = 0.26 and 0.157 calm water and wave maneuvering. Figure 7 shows the coordinate systems for the computations including ship-fixed Cartesian (x, y, z), and the earth-fixed Cartesian (x_o, y_o, z_o) and cylindrical (ρ, φ, z_o) coordinates. The earth-fixed coordinate system is assumed to be an inertial reference frame, where the fluid flow equations are solved, and the forces and moments are initially computed. The location and orientation of the ships with respect to the inertial earth-fixed system are described by linear translations and Euler angles. The rigid-body equations for ship motions are solved in the ship-fixed coordinate system, where the ship linear and angular velocities (u, v, w, p, q, r), and forces and moments (X, Y, Z, K, M, N) are transformed from the earth-fixed coordinates. Figure 8 shows the grid layout and distribution for the CFD simulations. The details of the CFD setup for Fr=0.26 are provided by Kim (2019) and the same approach was used for the Fr= 0.157. The CFD is for Re=3.61×10^6 (same as the IIHR experiments), actual propeller and coarse grid G3=12M. Results for G2=36M were also obtained; however, duration of the simulations is less, and the differences are not that large such that G3 is used for the validation and analysis. The CFDShip-Iowa results were also submitted to the SIMMAN 2021 workshop.

- The 3DoF force and moment balance was also assessed using the results form CFDShip-Iowa as follows:

$$\mathrm{m}(\dot{u} - vr + wq) \equiv X_{BH} + X_R + X_P$$
$$\mathrm{m}(\dot{v} - wp + ur) \equiv Y_{BH} + Y_R + Y_P$$
$$I_z\dot{r} + (I_y - I_x)pq \equiv N_{BH} + N_R + N_P$$

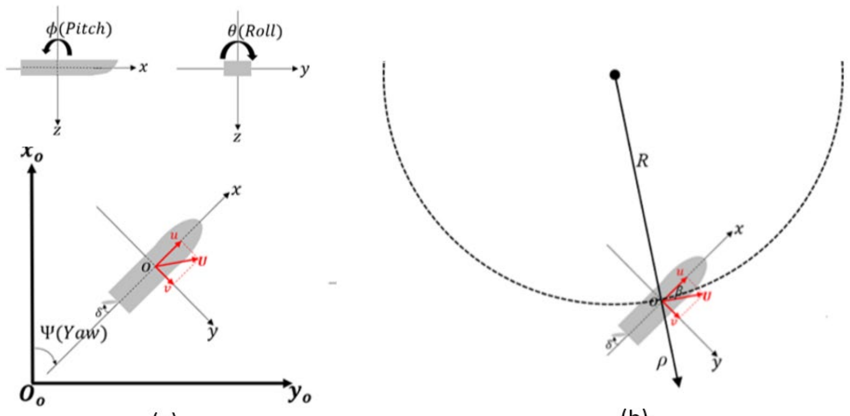

Figure 7. (a). Cartesian, (b) Cylindrical coordinates system

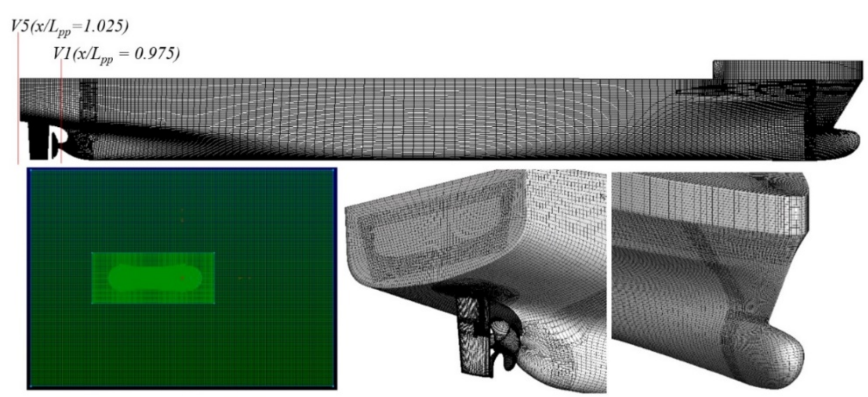

Figure 8. Grid distribution for CFD simulation of KCS

CFD Assessment and Validation of KCS Port and Starboard Turning Circles

- Figures 9 and 10 show the results including self-propulsion and propeller forces X_P and Y_P and moment N_P. The CFD has the same trends as the experiments. Interestingly and contrary to many persons' expectations the role of the propeller side force and moment are relatively small. These results validate the CFD for the assessment for the hull-propeller-rudder interaction as follows.

Figure 9. KCS nondimensional force and moment balance CFDShip-Iowa at Fr = 0.157

CFD Assessment and Validation of KCS Port and Starboard Turning Circles

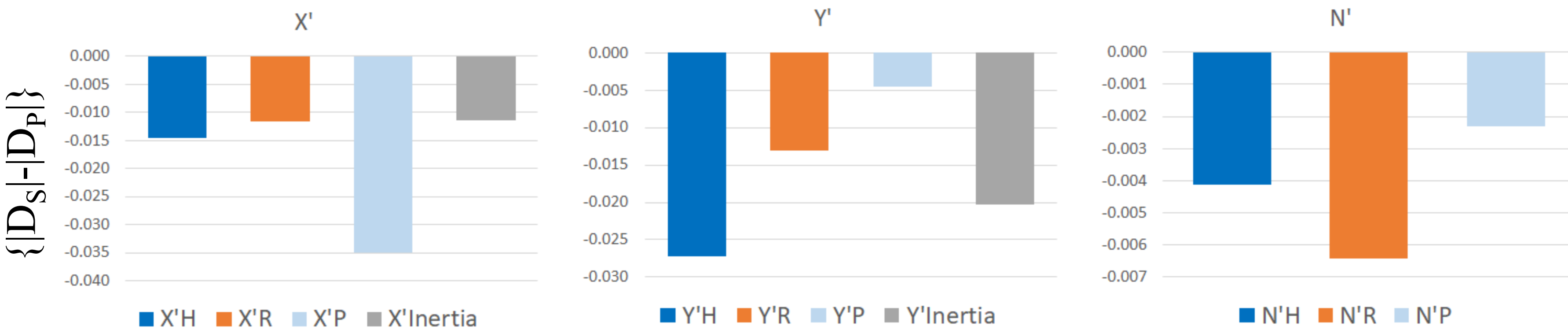

Figure 10. KCS nondimensional force and moment $\{|D_S|-|D_P|\}$ CFDShip-Iowa at Fr = 0.157

- CFD has same trends as the experiments, which validates CFD for hull-propeller-rudder interaction analysis

CFD Assessment of Hull-Propeller-Rudder Interaction

- Figure 11 shows the wave pattern for the self-propulsion and port and starboard turning circles at Fr=0.157. The amplitudes are about 3-4 times smaller compared to the Fr=0.26 results.

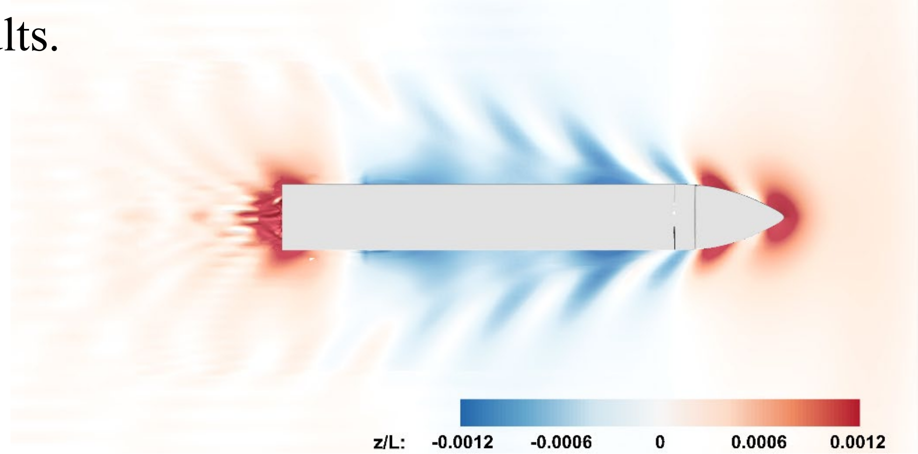

Free-surface deformation during steady state SP condition

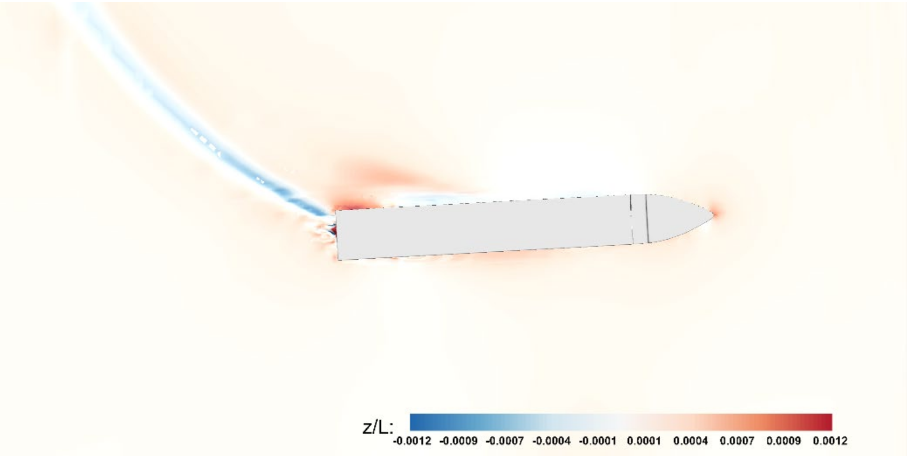

Free-surface deformation during steady state 35PSTC condition

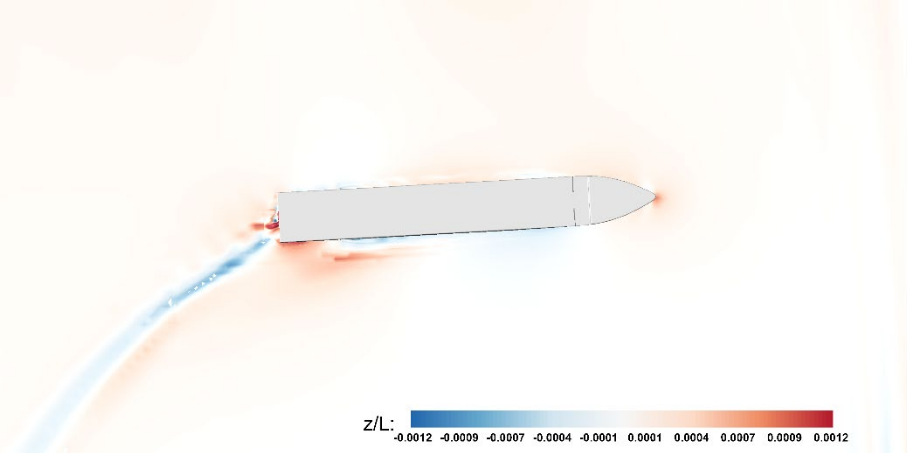

Free-surface deformation during steady state 35SBTC condition

Figure 11. Steady state wave pattern for self-propulsion and port and starboard turning at Fr=0.157

CFD Assessment of Hull-Propeller-Rudder Interaction

- Figure 12 shows the overall vortex structures for the steady state self-propulsion and port and starboard turning circles. The drift angle is positive on the starboard and negative on the port sides; therefore, when observing from the stern the hull vortices into the propeller are counterclockwise on starboard TC and clockwise on port TC vs. symmetric for self-propulsion, whereas propeller rotation is clockwise in all cases.

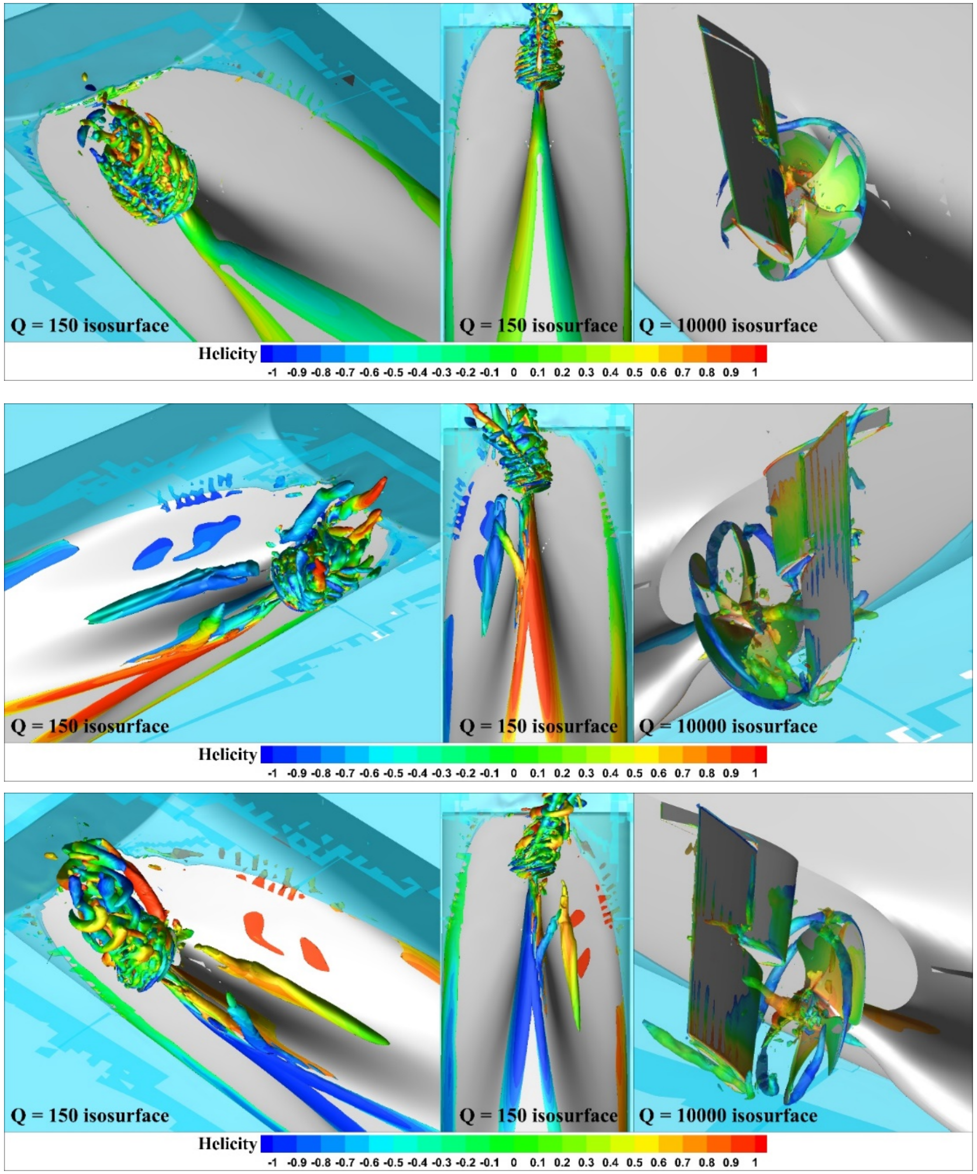

Vortical Structure during steady state SP condition

Vortical Structure during steady state 35PSTC condition

Vortical Structure during steady state 35SBTC condition

Figure 12. Vortex Structures during steady state condition at Fr=0.157

CFD Assessment of Hull-Propeller-Rudder Interaction

- Figure 13 shows the wide view propeller inflow for the steady state self-propulsion and port and starboard turning circles, including with propeller and rudder, without propeller and with rudder and without propeller and rudder. The propeller induced velocities show interactions with the hull-induced vortices, whereas the effects of the rudder are minimal. (averaged over 14 blade rotation)

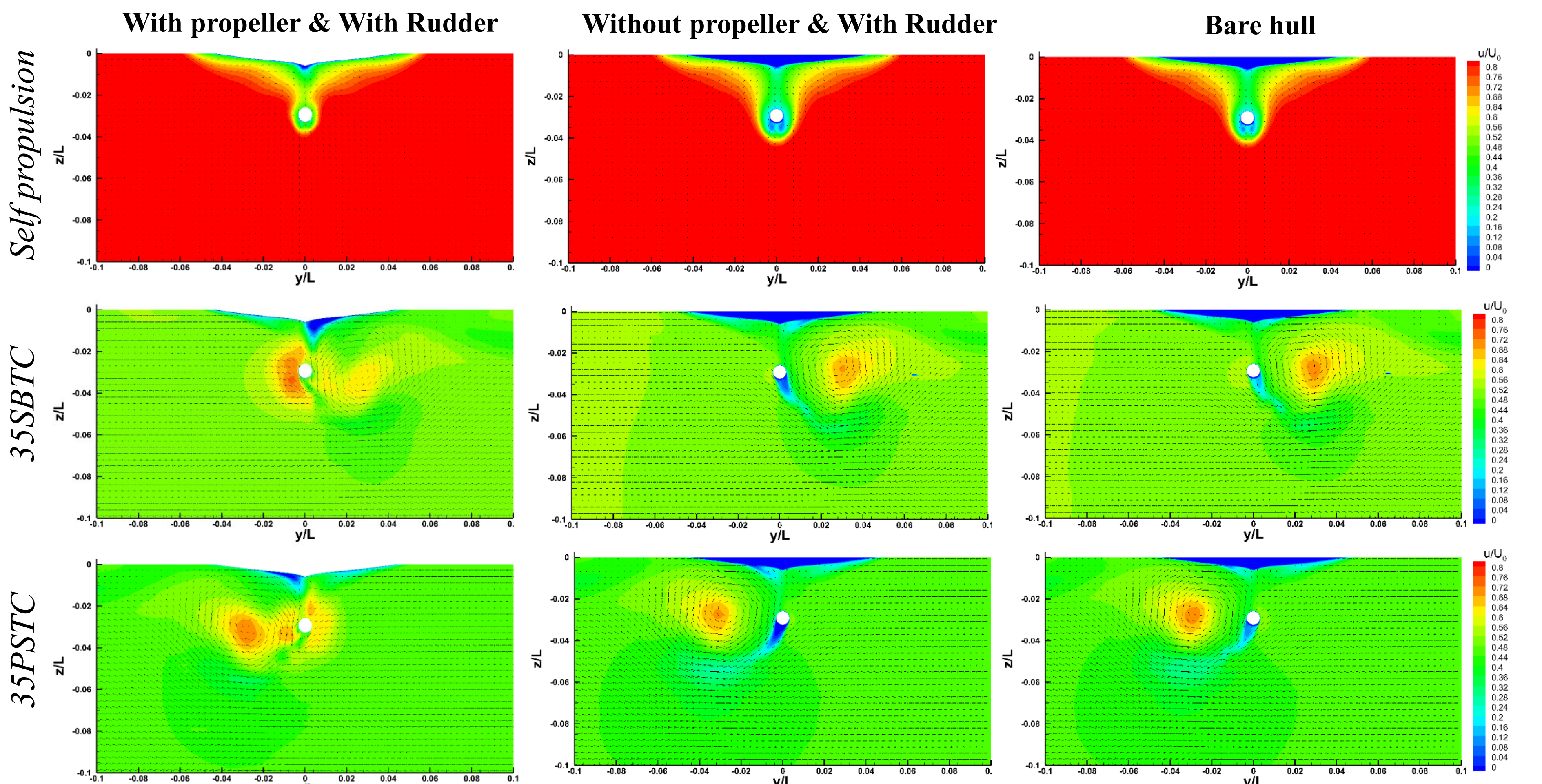

Figure 13. V1(x/L_{pp} = 0.975) section during steady state (with propeller & Rudder) at Fr =0.157.

CFD Assessment of Hull-Propeller-Rudder Interaction

- Figures 14, 15, and 16 show the propeller inflow and rudder wake for self-propulsion and starboard and port turning, respectively, including with propeller and rudder, without propeller and with rudder and without propeller and rudder, which highlight the wide view trends. (averaged over 14 blade rotations)

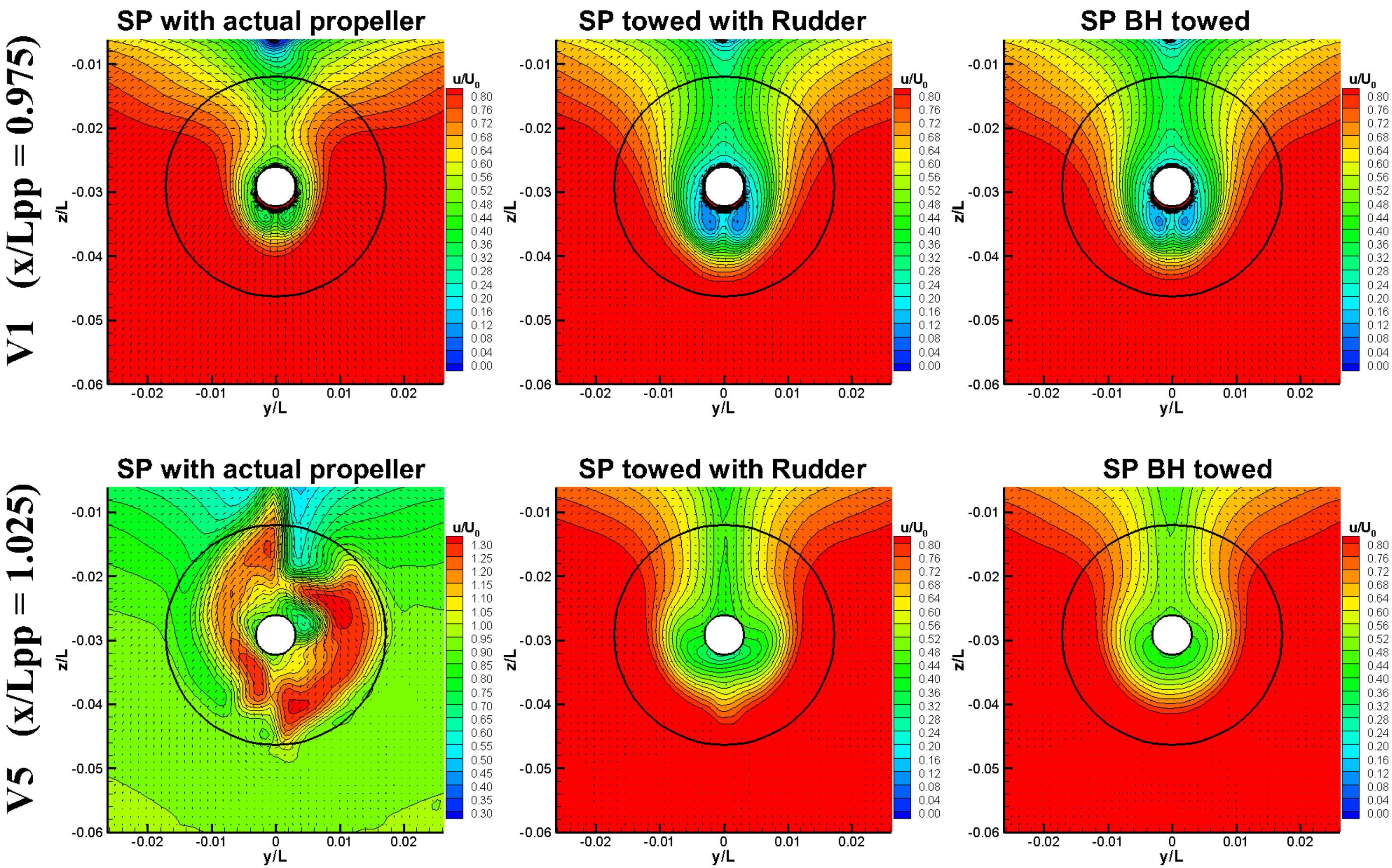

Figure 14. Averaged propeller inflow for steady state SP condition at Fr=0.157

CFD Assessment of Hull-Propeller-Rudder Interaction

- Figures 14, 15, and 16 show the propeller inflow and rudder wake for self-propulsion and starboard and port turning, respectively, including with propeller and rudder, without propeller and with rudder and without propeller and rudder, which highlight the wide view trends. (averaged over 14 blade rotations)

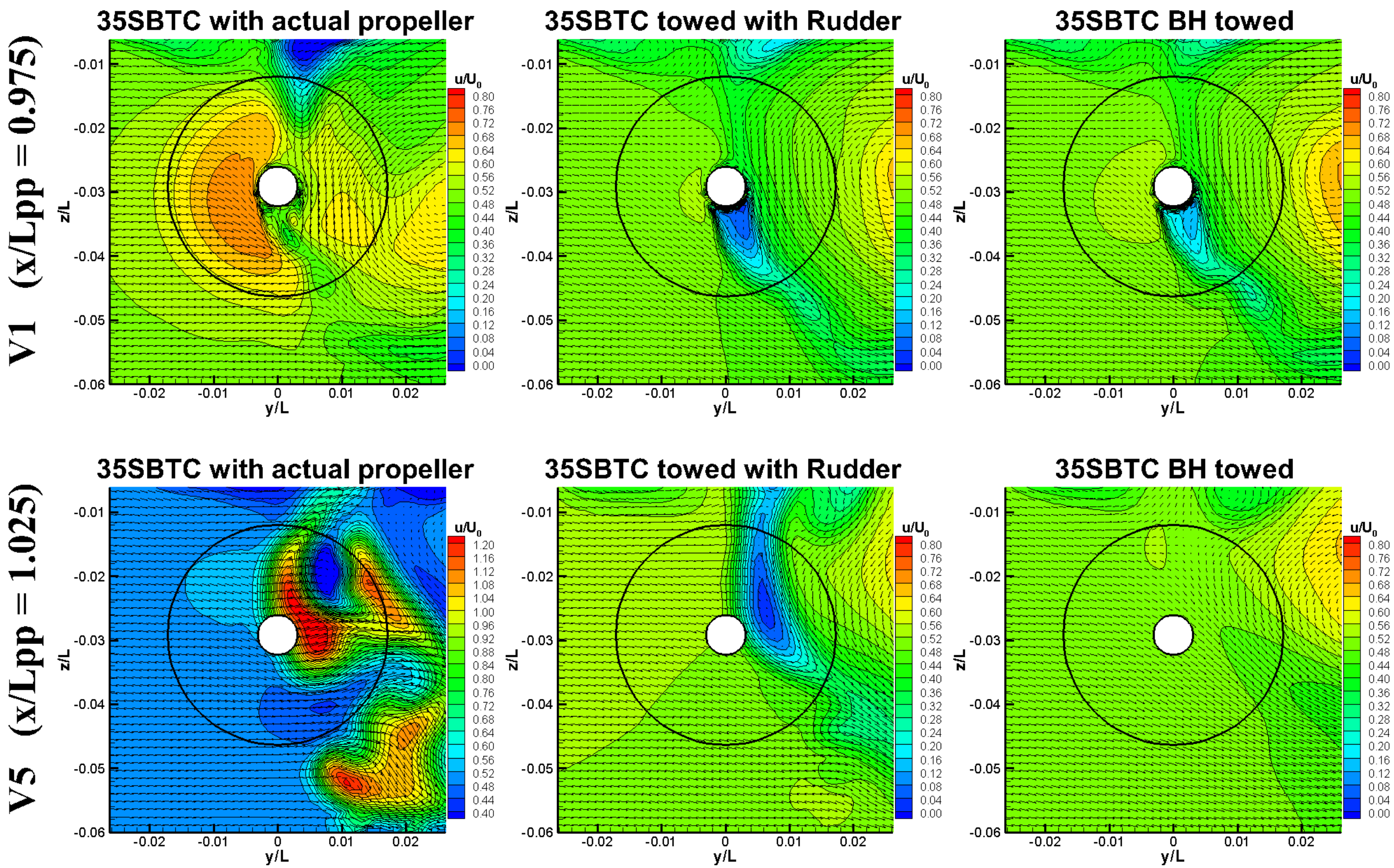

Figure 15. Averaged propeller inflow for steady state 35SBTC condition at Fr=0.157

CFD Assessment of Hull-Propeller-Rudder Interaction

- Figures 14, 15, and 16 show the propeller inflow and rudder wake for self-propulsion and starboard and port turning, respectively, including with propeller and rudder, without propeller and with rudder and without propeller and rudder, which highlight the wide view trends. (averaged over 14 blade rotations)

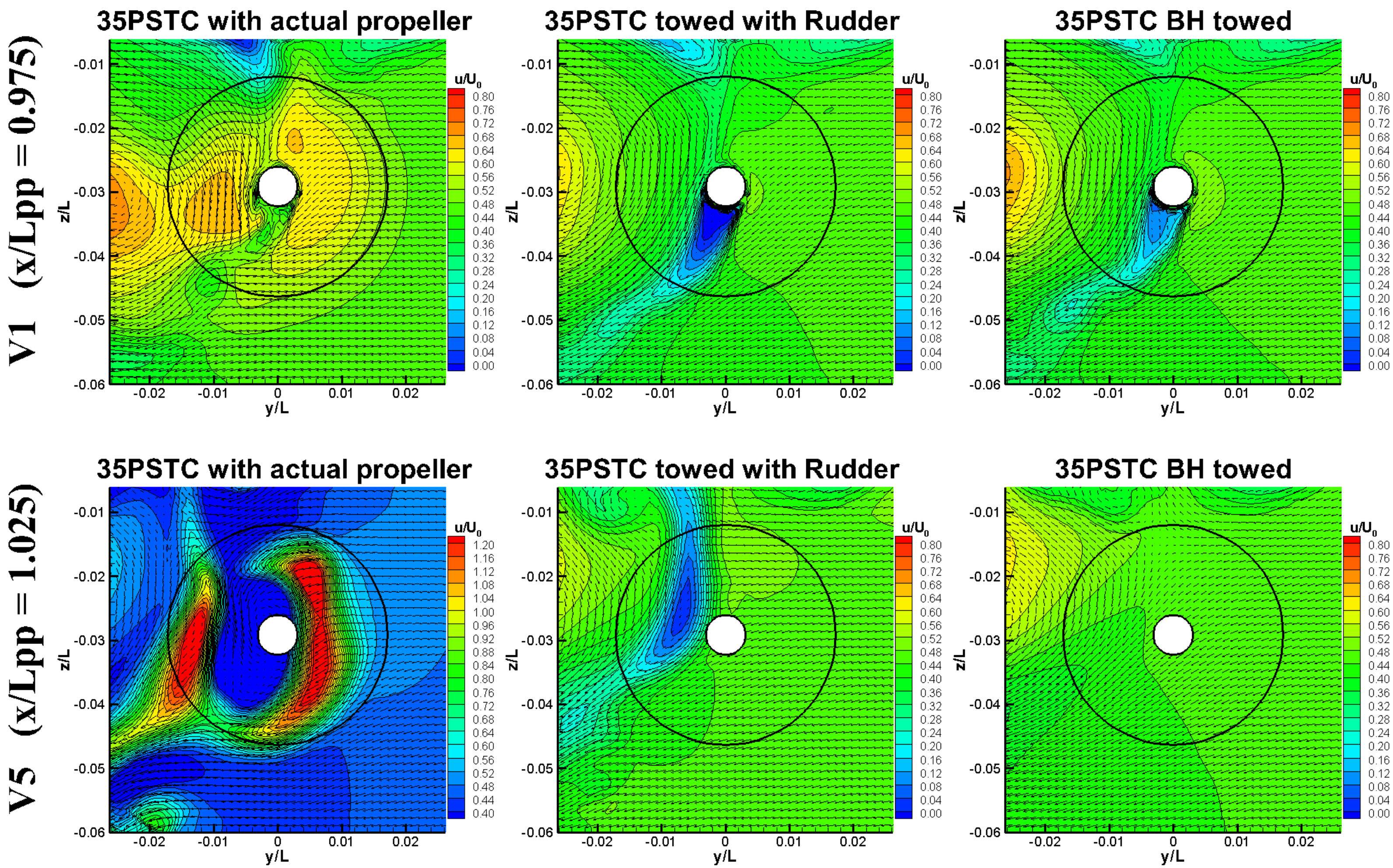

Figure 15. Averaged propeller inflow for steady state 35PSTC condition at Fr=0.157

CFD Assessment of Hull-Propeller-Rudder Interaction

- Table 4 provides the wake coefficients for the propeller inflow. Note that the wake coefficients are based on total velocity including the propeller induced velocities. For self-propulsion, the wake fraction is reduced substantially without the propeller and slightly increased by the rudder. The wake fraction is larger for starboard than port turning. The inboard vs. outboard, i.e., rudder vs. non-rudder side always has smaller wake fraction; however, the effects of the rudder are relatively small, i.e., about 5%. The upper vs. lower wake coefficients are smaller for self-propulsion and larger for turning.

Table 4. Wake coefficient at V1 section (Fr = 0.157)

	SP	35PSTC			35SBTC		
With Propeller & Rudder	0.758	0.563			0.583		
		Inboard	**Outboard**	**In/Out**	**Inboard**	**Outboard**	**In/Out**
		0.549	0.577	0.951	0.529	0.638	0.829
		Top	**Bottom**	**Top/Bottom**	**Top**	**Bottom**	**Top/Bottom**
		0.554	0.572	0.969	0.563	0.603	0.934
With Rudder No propeller	0.586	0.396			0.444		
		Inboard	**Outboard**	**In/Out**	**Inboard**	**Outboard**	**In/Out**
		0.352	0.441	0.798	0.397	0.491	0.809
		Top	**Bottom**	**Top/Bottom**	**Top**	**Bottom**	**Top/Bottom**
		0.424	0.369	1.149	0.465	0.422	1.102
Bare Hull	0.606	0.418			0.468		
		Inboard	**Outboard**	**In/Out**	**Inboard**	**Outboard**	**In/Out**
		0.383	0.453	0.845	0.429	0.506	0.848
		Top	**Bottom**	**Top/Bottom**	**Top**	**Bottom**	**Top/Bottom**
		0.442	0.395	1.119	0.489	0.447	1.094

CFD Assessment of Hull-Propeller-Rudder Interaction

- Table 5 lists EFD effective wake coefficient obtained by thrust identity method for IIHR and HU.

- Figure 17 provides the open water curves for the KP505 propeller. The current self-propulsion J ≈ 0.8 is less than optimum since at the model point and propeller was designed for full scale self-propulsion point which is as per NMRI self-prolusion experiments J = 0.93. Table 6 provides the J values for the experiments and CFD, which shows that J is reduced for turning circles, especially for port turning.

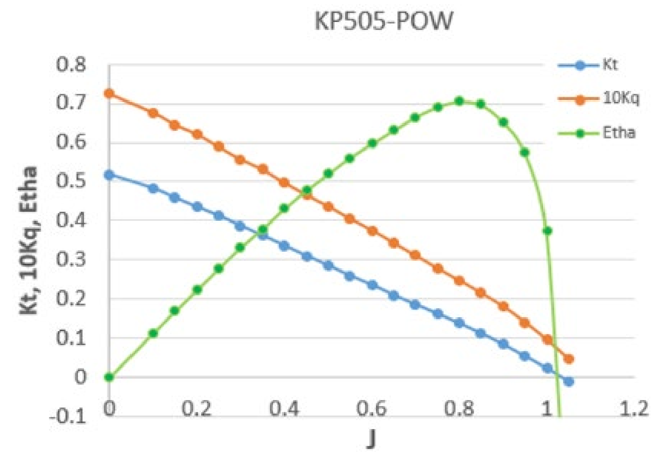

Figure 17. KCS Propeller open water curve (Geometry: KP505)

Table 5. EFD effective wake coefficient obtained by thrust identity method (Fr = 0.157)

	SP	35PSTC	35SBTC
HU	-	0.711	0.605
IIHR	0.675	0.805	0.739

Table 6. Steady state J_B (=U/nD) values for each case

Case	Starboard (D_S)	Port side (D_P)	Mean $=(\lvert D_S\rvert+\lvert D_P\rvert)/2$	$\Delta D=\lvert D_S\rvert-\lvert D_P\rvert$	ΔD%Mean
HU (Fr = 0.157)	0.3724	0.3514	0.3619	0.02102	5.81
IIHR (Fr = 0.157)	0.3693	0.3362	0.3528	0.03309	9.38
IIHR (Fr = 0.26)	0.3480	0.3200	0.3341	0.02742	8.21
CFD (Fr = 0.26)	0.4431	0.4322	0.4377	0.0109	2.49

CFD Assessment of Hull-Propeller-Rudder Interaction

- Figure 18 shows that the propeller is more heavily loaded for turning compared self-propulsion, especially for port turning. The loss in propeller efficiency as per t' correlation induces speed loss. The KP505 propeller uses NACA66 blade sections, which for Re $\cong 10^6$ have the maximum C_L/C_D when the angle of attack is 3.25°, which is assumed to be the design value for full scale operation. Figure 19 shows the blade section able of attack at the 70% radius vs. propeller blade angle for the self-propulsion and starboard and port turning. The average angle of attack is 4.65° for self-propulsion; 8.60° for port turning; and 7.84° for starboard turning. The larger value for self-propulsion than the design value is due to model vs. ship point, whereas the larger values for turning are due to the hull induced vortices and hull-propeller interaction, especially for the port turning.

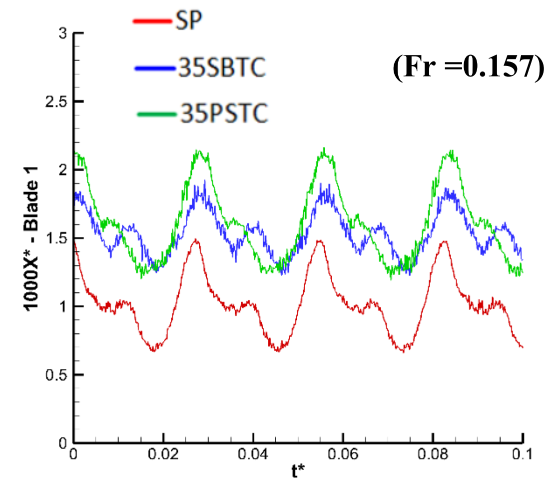

Figure 18. Hydrodynamic X force of a single blade during SP, 35SB TC(TC+35) and 35PSTC (TC-35) in steady state part (phase is mat ched with SP and Turning)

- KP505 propeller uses NACA66. When t Re $\cong 10^6$,
  Max Cl/Cd of NACA66 can be achieved when AoA is ***3.25 deg***.

- Average AoA (Fr = 0.157):
  SP: 4.65deg; 35PSTC: 8.60deg; and 35SBTC: 7.84deg

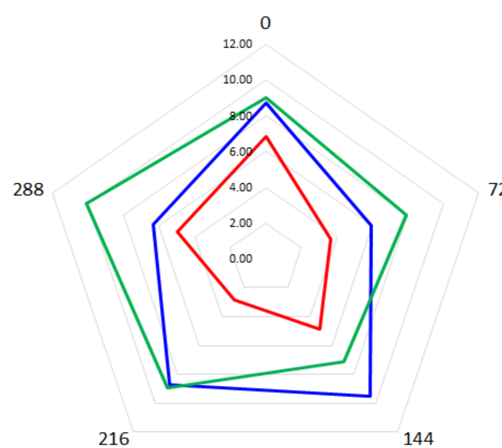

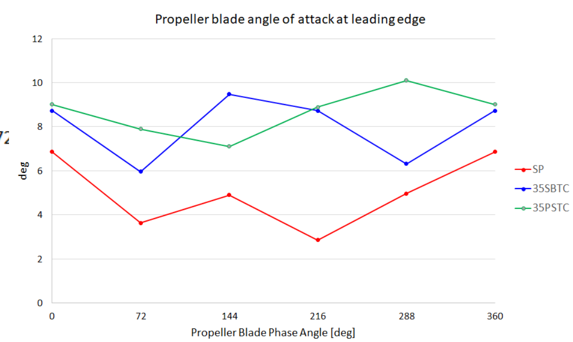

Figure 19. Propeller Blade Angle of attack comparison at 70% radius at Fr = 0.157.

CFD Assessment of Hull-Propeller-Rudder Interaction

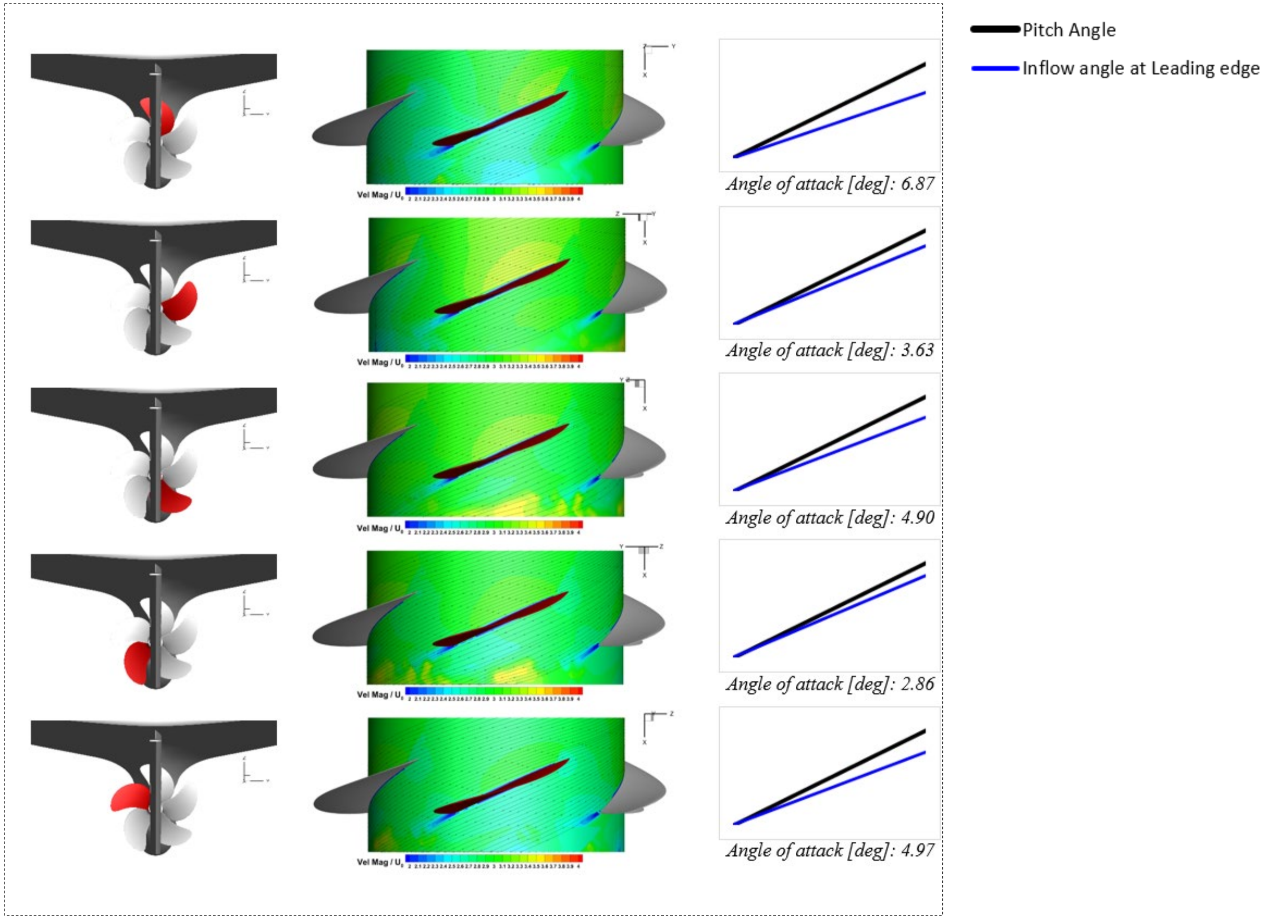

Figure 20. Propeller Blade Angle of attack at 70% radius of SP (Fr#: 0.157)

CFD Assessment of Hull-Propeller-Rudder Interaction

Pitch Angle
Inflow angle at Leading edge

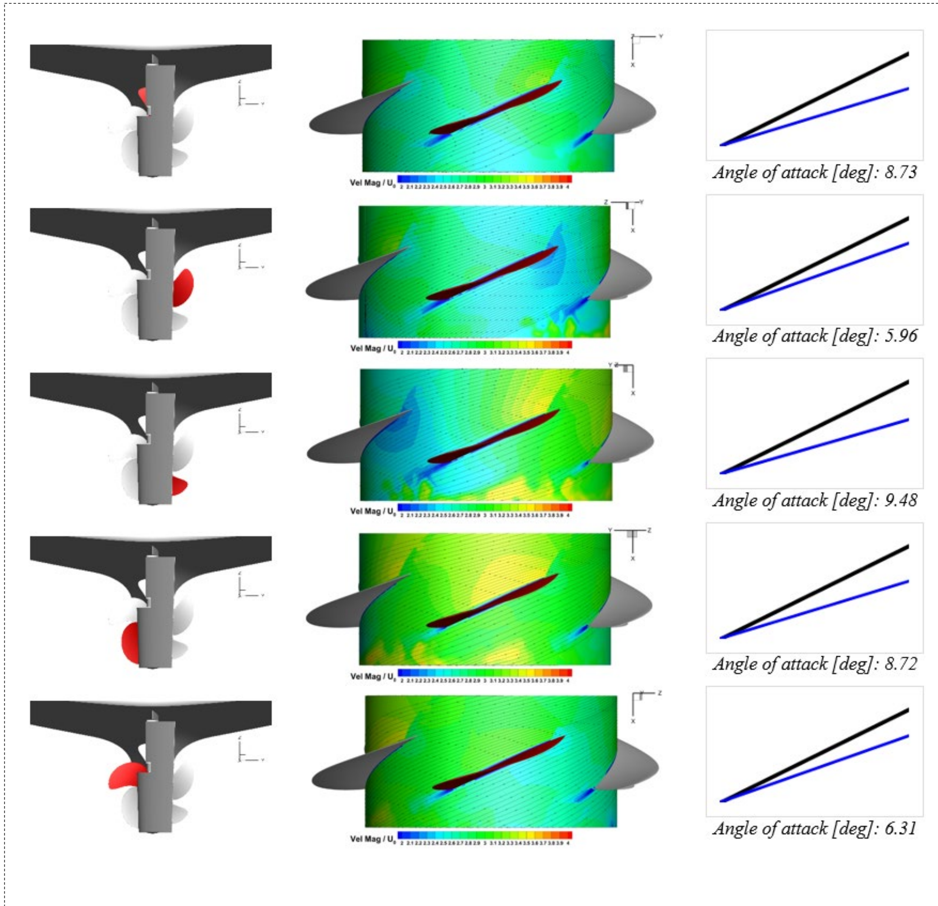

Figure 21. Propeller Blade Angle of attack at 70% radius of 35SBTC (Fr#: 0.157)

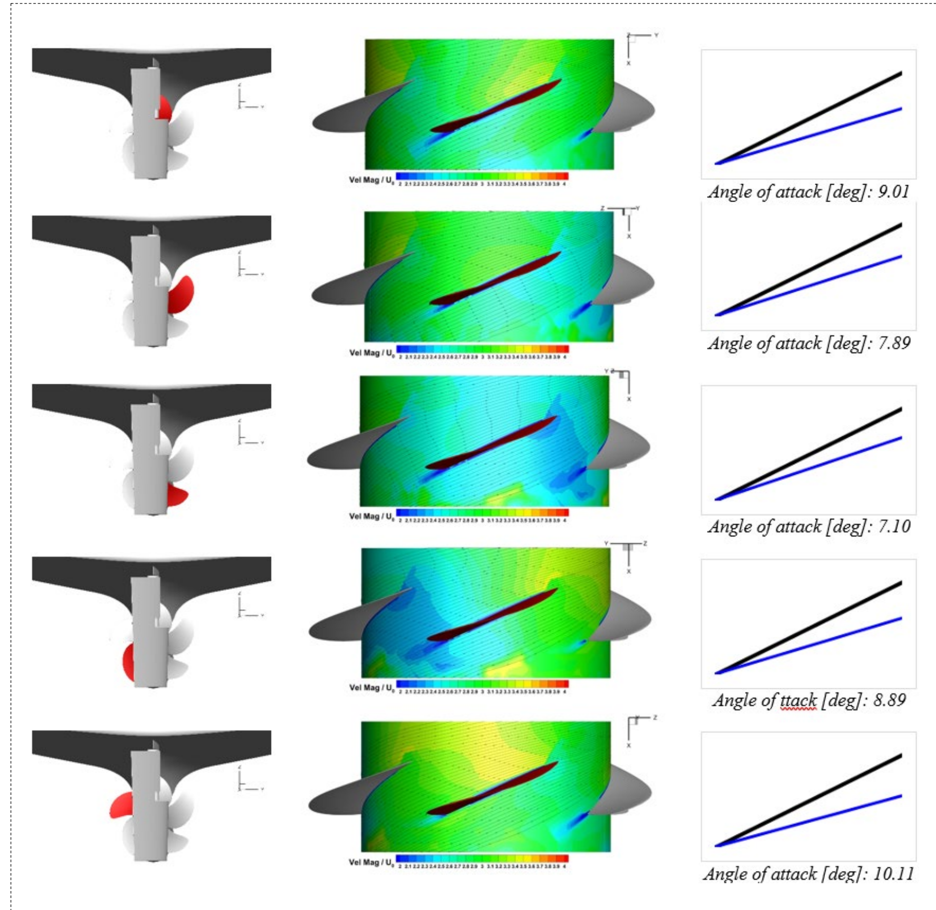

Figure 22. Propeller Blade Angle of attack at 70% radius of 35PSTC (Fr#: 0.157)

CFD Assessment of Hull-Propeller-Rudder Interaction

- The results explain the hull-propeller-rudder interaction for self-propulsion and port and starboard turning circles. The experimental and CFD circular motion equations (5) and (7) can be interpreted as follows. For steady-state circular motion of a ship with a constant speed U and radius R, Eq. (7) can be simplified and rewritten in the cylindrical system (see Figure 7),

$$mU^2/R = \rho_{BH} + \rho_R + \rho_P$$
$$0 \equiv N_{BH} + N_R + N_P$$

where $U = \sqrt{u^2 + v^2}$, and $\rho = \sqrt{X^2 + Y^2}$. The primary state variables are the u and v components of the ship velocity (with respect to the earth-fixed frame) expressed in the ship-fixed coordinate system (x, y, z) since the yaw angular velocity $r = \sqrt{u^2 + v^2}/R$. The force balance can be explained in the non-inertial rotating frame, where the centrifugal force mU^2/R due to the inertia is balanced by the hydrodynamic ship hull, propeller and rudder forces, resulting in the steady state equilibrium condition with the key outcome of drift angle $\beta = tan^{-1}(v/u)$, which induces the hull vortices, propeller inflow and loss in efficiency and speed loss. The N equation plays a passive role in simply balancing the yaw and rudder moments. The key physical mechanisms are the centrifugal force, and hull-propeller interaction, whereas the propeller side force and yaw moment and rudder play largely passive role notwithstanding the rudder inducing the entire event.

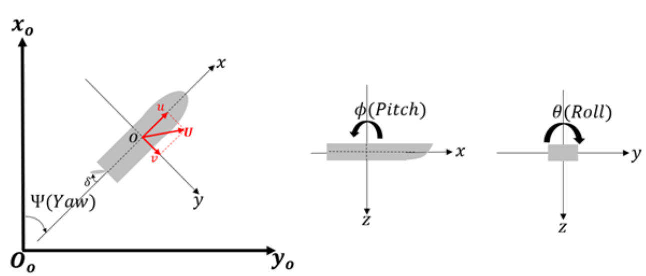

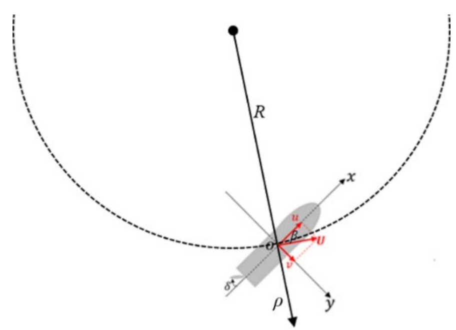

Figure 7. Coordinate systems: (a). Cartesian coordinates, (b) Cylindrical coordinates.

Overall Conclusions and Prognosis Maneuvering In waves

- Experiments and CFD are combined to explain the physics of the KCS hull-propeller-rudder interaction for turning circles and the reason for differences between port and starboard turning. The t' correlation is promising for scaling model size and both course keeping and maneuvering in clam water and waves; but needs more study for model size and effects of different maneuvers. The MMG rudder model is useful but needs more study for general applicability. The X, Y, N force and moment balance helps to explain maneuvering and differences port vs. starboard maneuvers. The CFD shows the same X, Y, N force and moment balance as the experiments and completes the explanation of the details of the hull-propeller-rudder interaction for port vs. starboard maneuvering. The propeller inflow is different from the self-propulsion condition due to drift-angle induced hull vortices with similar trends for both port and starboard, but larger magnitudes for port. The propeller is more heavily loaded for turning compared with self-propulsion, especially for port turning. The loss in propeller efficiency as per t' correlation induces speed loss. The results explain the hull-propeller-rudder interaction for self-propulsion and port and starboard turning circles. The experimental and CFD circular motion equations (5) and (7) can be interpreted as follows. The primary state variables are the u and v components of the ship velocity expressed in the ship-fixed coordinate system (x, y, z) since the yaw angular velocity $r = \sqrt{u^2 + v^2}/R$. The force balance can be explained in the non-inertial frame, where the centrifugal force mU^2/R due to the inertia is balanced by the hydrodynamic ship hull, propeller and rudder forces, resulting in the steady state equilibrium condition with the key outcome of drift angle $\beta = tan^{-1}(v/u)$, which induces the hull vortices, propeller inflow and loss in efficiency and speed loss. The N equation plays passive role in simply balancing the yaw and rudder moments. The key physical mechanisms are the centrifugal acceleration, and hull-propeller interaction, whereas the propeller side force and yaw moment and rudder play largely passive role notwithstanding the rudder inducing the entire event. It is hypothesized the similar physics albeit subject to transient effects and alternating semi-circular events are exhibited for zig-zag maneuvers.

- Extensions for maneuvering in waves in progress and continued collaboration AVT-348 and CNR-INM including use of CFDShip-Iowa and data-driven/mathematical-physics-based models following extensions current approach for 6DoF, waves, more severe conditions and different maneuvers. Previous IIHR research of system identification (Araki et al., 2012) and machine learning (Dogan et al., 2020) should be helpful.

Overall Conclusions and Prognosis Maneuvering In waves

- Extensions for maneuvering in waves in progress

Stern, F. (Co_PI: Sanada,Y.)	**Global and Local Flow Modeling and Validation Experiments for Free-running ONRT Surface Combatant Maneuvering in Waves**	**Office of Naval Research**	**10/01/2020 - 09/30/2023**	**awarded**
Stern, F. (Co_PI: Sanada,Y.)	Global and Local Flow Measurement System for Modeling and Validation Experiments for Free-running ONRT Surface Combatant Maneuvering in Waves	Office of Naval Research	02/01/2021 – 01/31/2022	**awarded**

- Acquisition of equipment is in progress to support global and local flow modeling and validation experiments for free-running ONR Tumblehome (ONRT) surface combatant maneuvering in waves. The equipment includes: (1) load cells and amplifiers for measuring propeller side force and rudder axial and side force and yaw moment, and metal propellers for enhanced volumetric local flow velocity measurements; (2) 6DoF soft spring mount (surge, sway and yaw linear motor) for measuring horizontal wave drift forces and moment during the model maneuvers; and (3) instrumentation for increased accuracy of the tracking system and the wave maker controller; and lenses for increased 4DPTV spatial resolution.

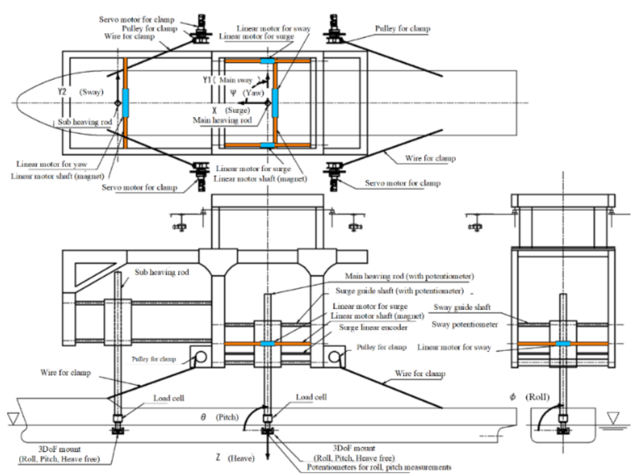

6DoF Mount for Wave Drift Force Measurements (Orange: Linear motor shaft with linear encoder, Blue: Linear motor (Movable part))

Appendix

KCS nondimensional force balance IIHR turning at Fr = 0.26

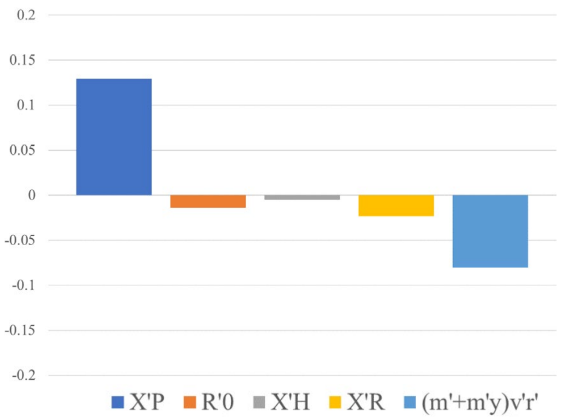

X(Starboard)

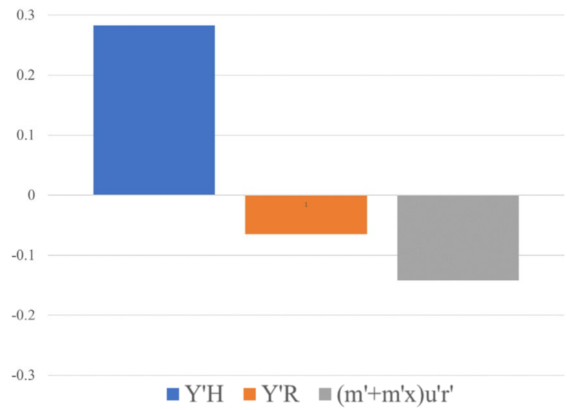

Y(Starboard)

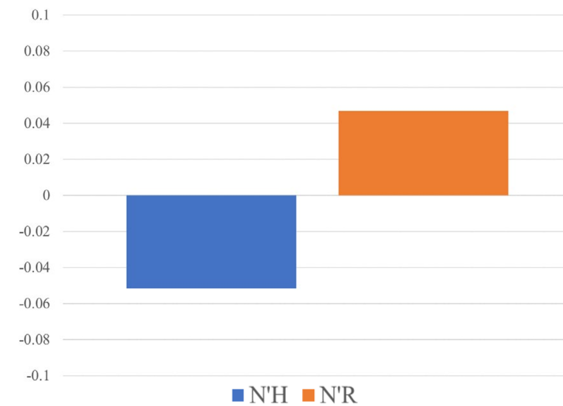

N(Starboard)

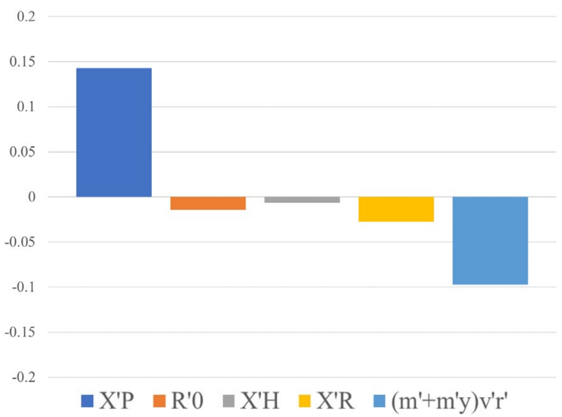

X(Port)

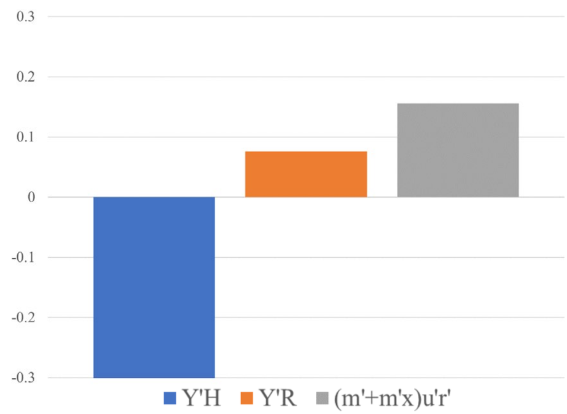

Y(Port)

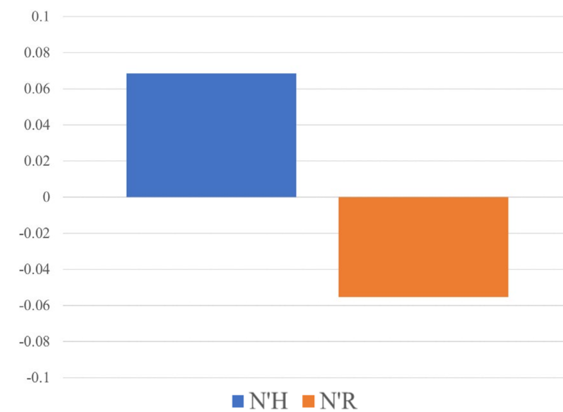

N(Port)

- IIHR Fr=.26 has same trends as Fr=.157

Appendix

Nondimensional force ΔD%Mean comparison between HU and IIHR at Fr=0.157

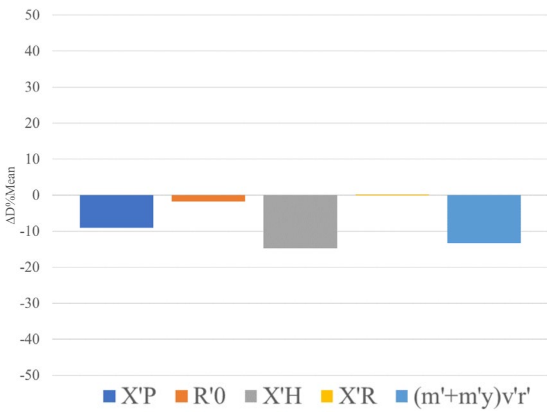

X(HU)

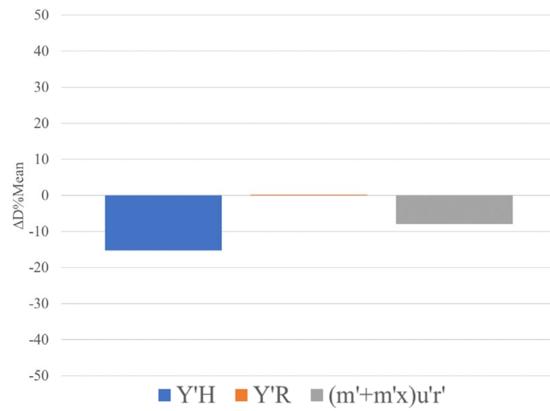

Y(HU)

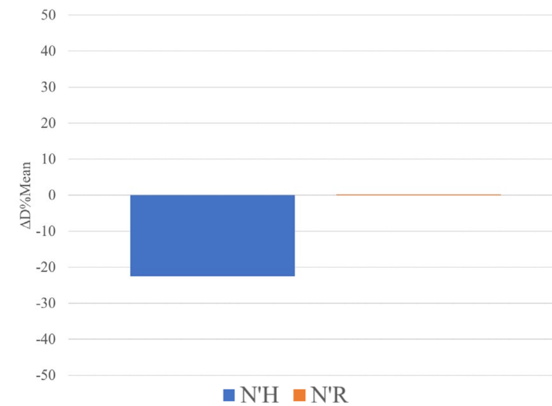

N(HU)

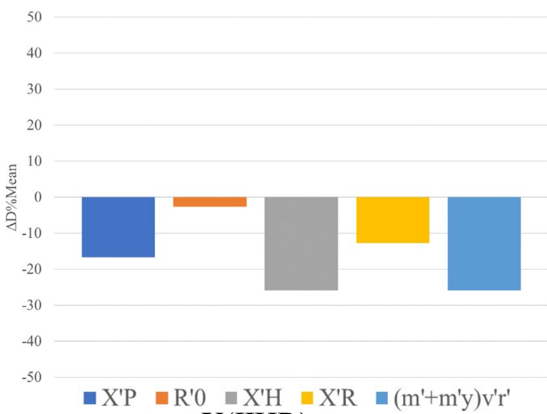

X(IIHR)

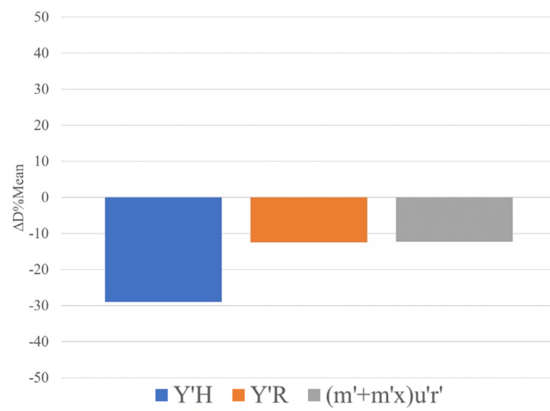

Y(IIHR)

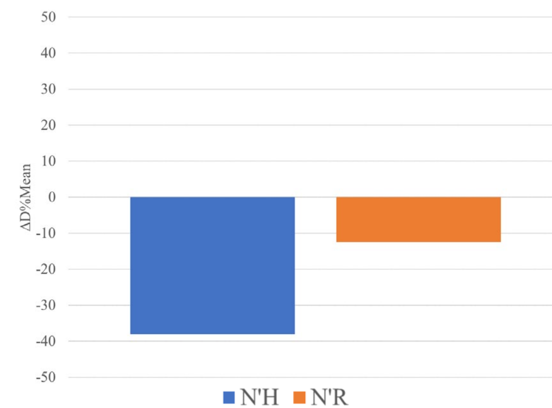

N(IIHR)

- All force and moment components larger magnitudes for port vs. starboard.

Appendix

IIHR nondimensional force ΔD%Mean at Fr=0.26

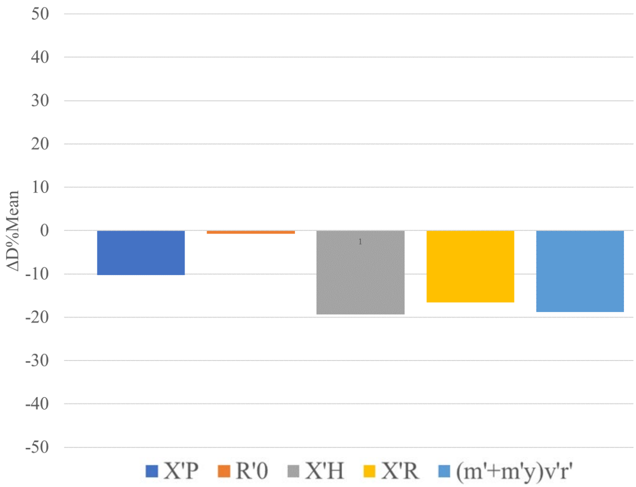

X(IIHR)

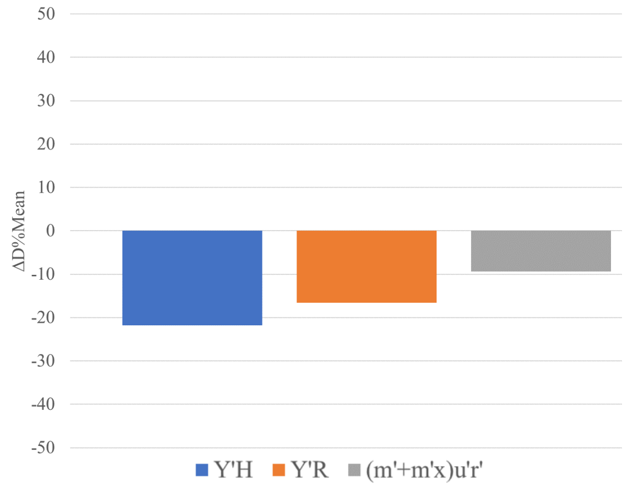

Y(IIHR)

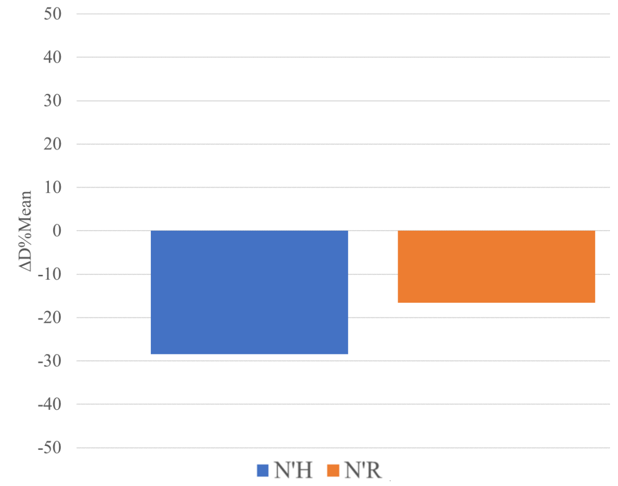

N(IIHR)

- Fr=.26 has same trends Fr=.157, i.e., all force and moment components larger magnitudes for port vs. starboard.

Appendix

CFD Assessment and Validation of KCS Port and Starboard Turning Circles Fr=0.26

$$m(\dot{u} - vr + wq) \equiv X_{BH} + X_R + X_P$$
$$m(\dot{v} - wp + ur) \equiv Y_{BH} + Y_R + Y_P$$
$$I_z\dot{r} + (I_y - I_x)pq \equiv N_{BH} + N_R + N_P$$

Self propulsion

35SBTC

35PSTC

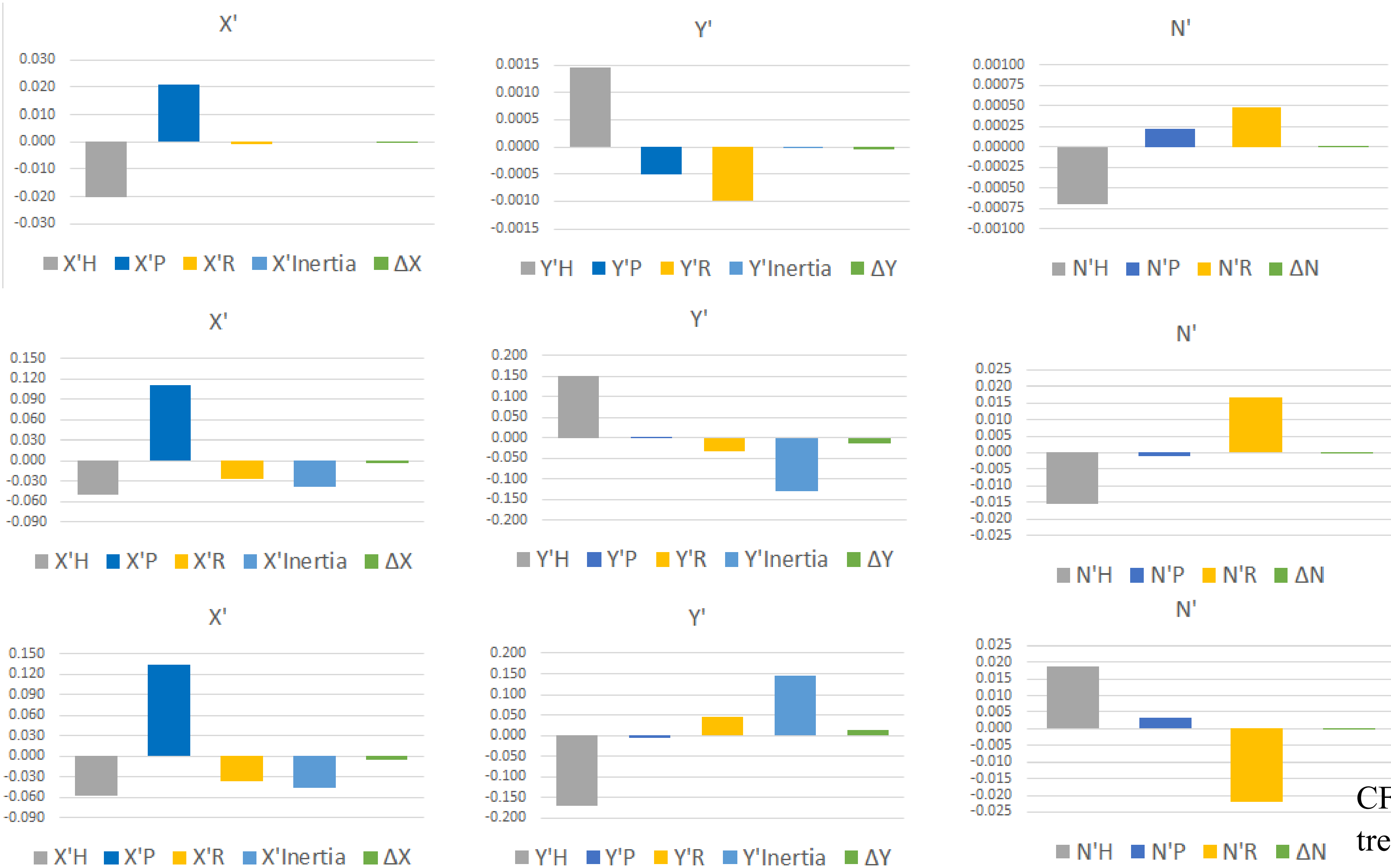

CFD has same trends as the experiments

Appendix

CFDShip-Iowa v4.5 nondimensional force ΔD%Mean at Fr = 0.26

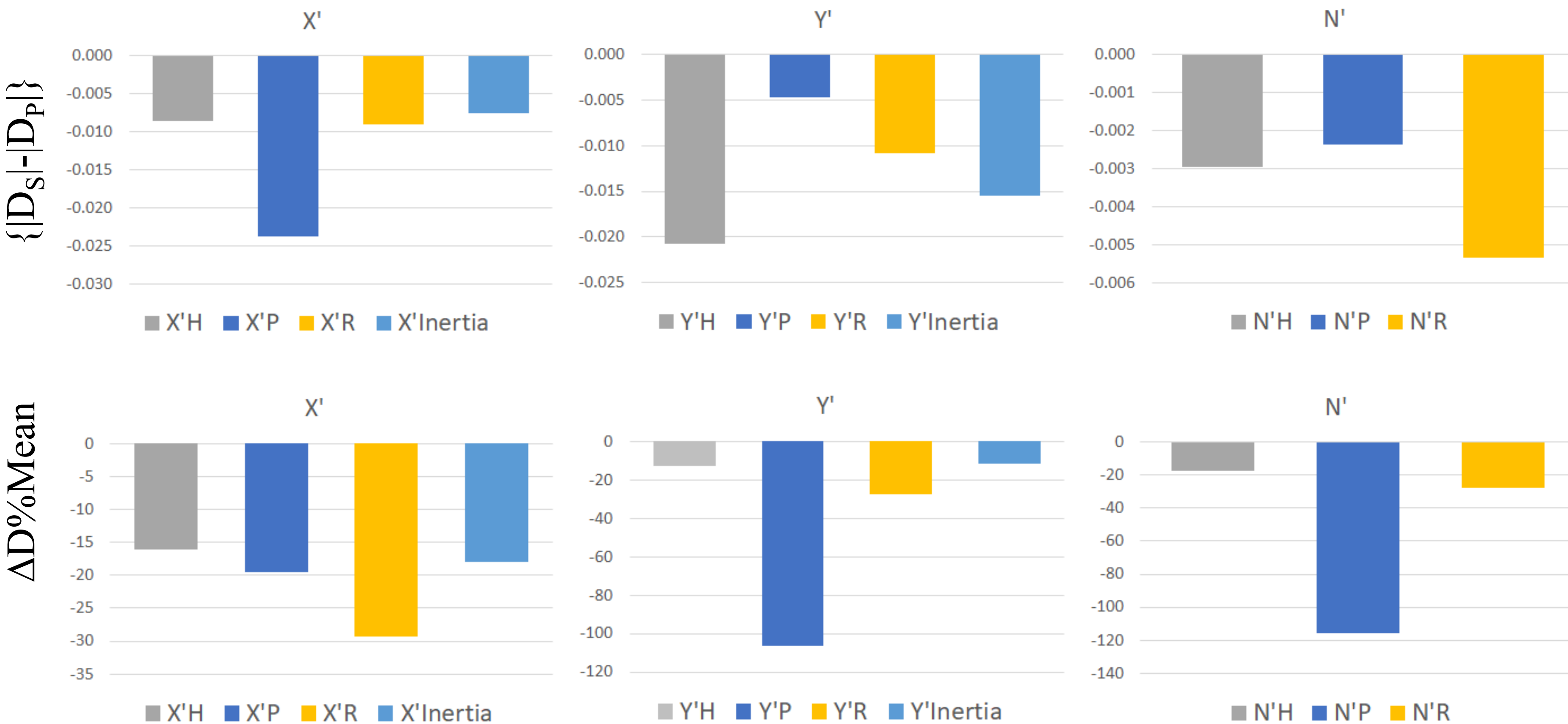

- CFD has same trends as the experiments

Appendix

CFD Assessment of Hull-Propeller-Rudder Interaction (Fr = 0.26)

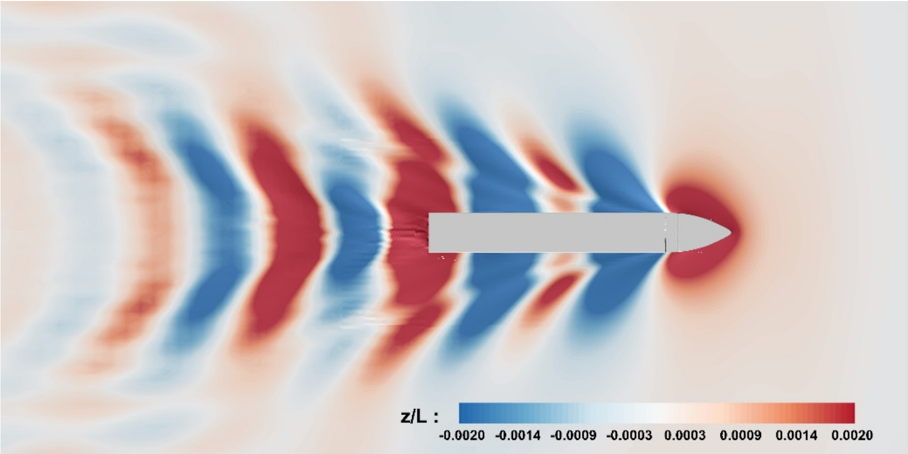

Free-surface deformation during steady state SP condition

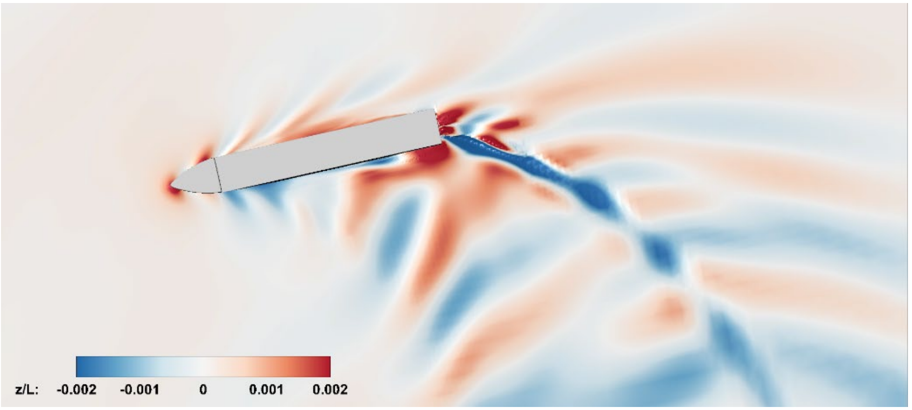

Free-surface deformation during steady state 35PSTC condition

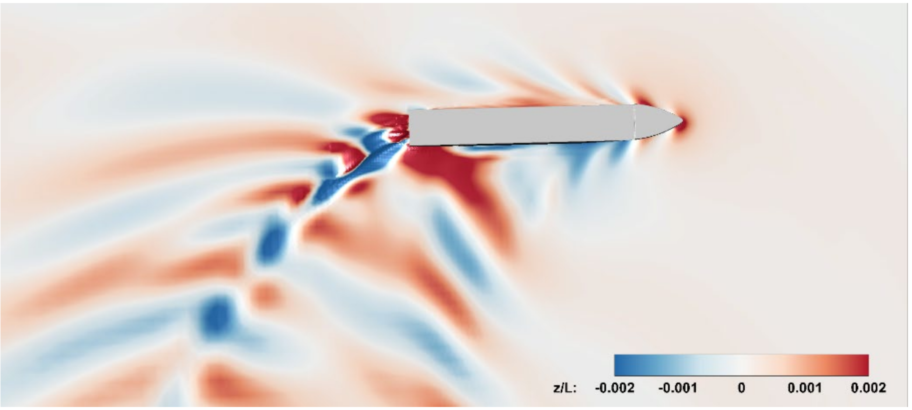

Free-surface deformation during steady state 35SBTC condition

Appendix

CFD Assessment of Hull-Propeller-Rudder Interaction (Fr = 0.26)

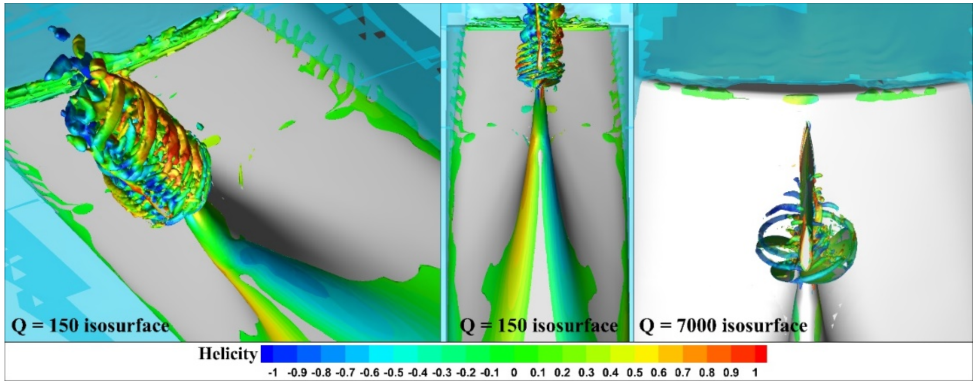

Vortical Structure during steady state SP condition

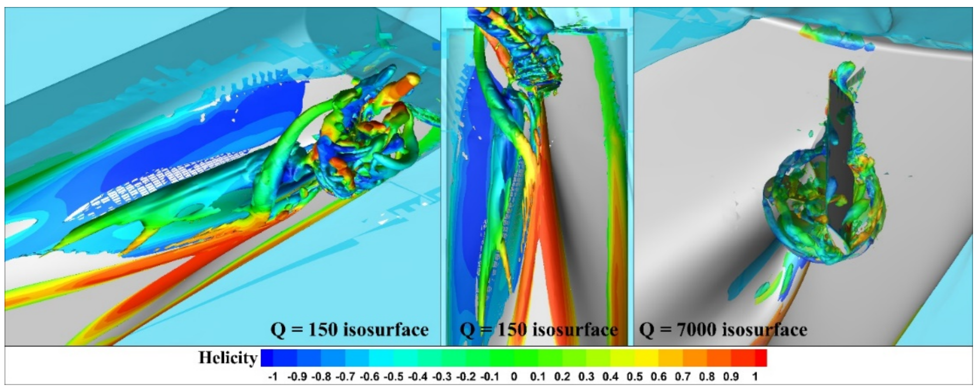

Vortical Structure during steady state 35PSTC condition

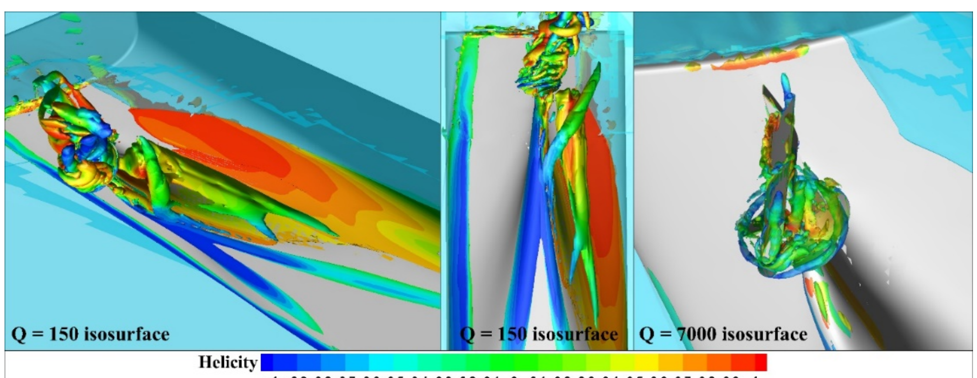

Vortical Structure during steady state 35SBTC condition

Appendix

Wide view of u/U_0 (left) and axial Vorticity(right) at x/ L = 0.975 section. ***(averaged over 14 blade rotation)***

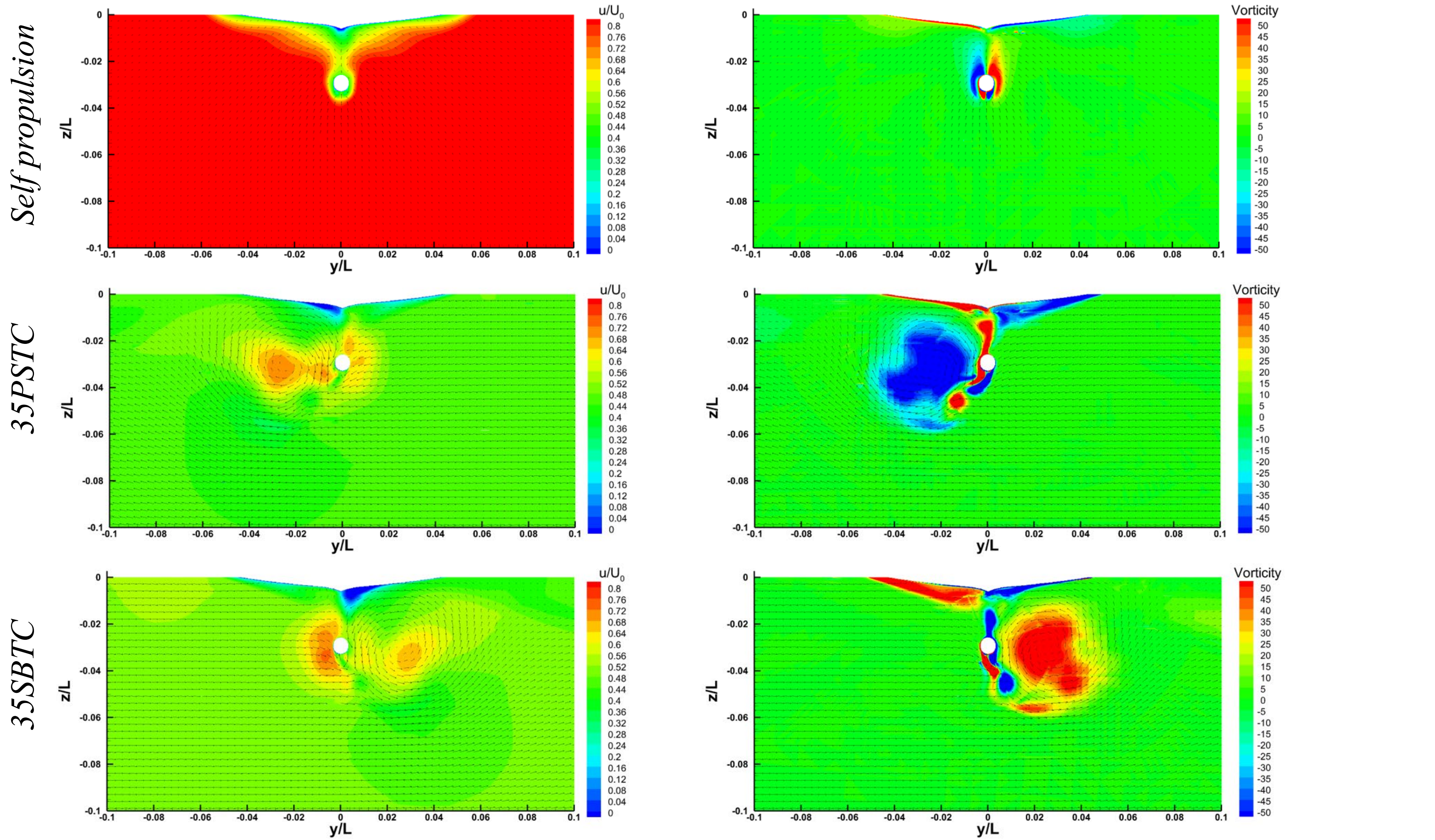

- Drift angle is positive on the starboard and negative on the port sides; therefore, hull vortices into propeller are counterclockwise on starboard and clockwise on port, whereas propeller always clockwise.

Appendix

Averaged propeller inflow at x/ L= 0.975 section. *(averaged over 14 blade rotation)*

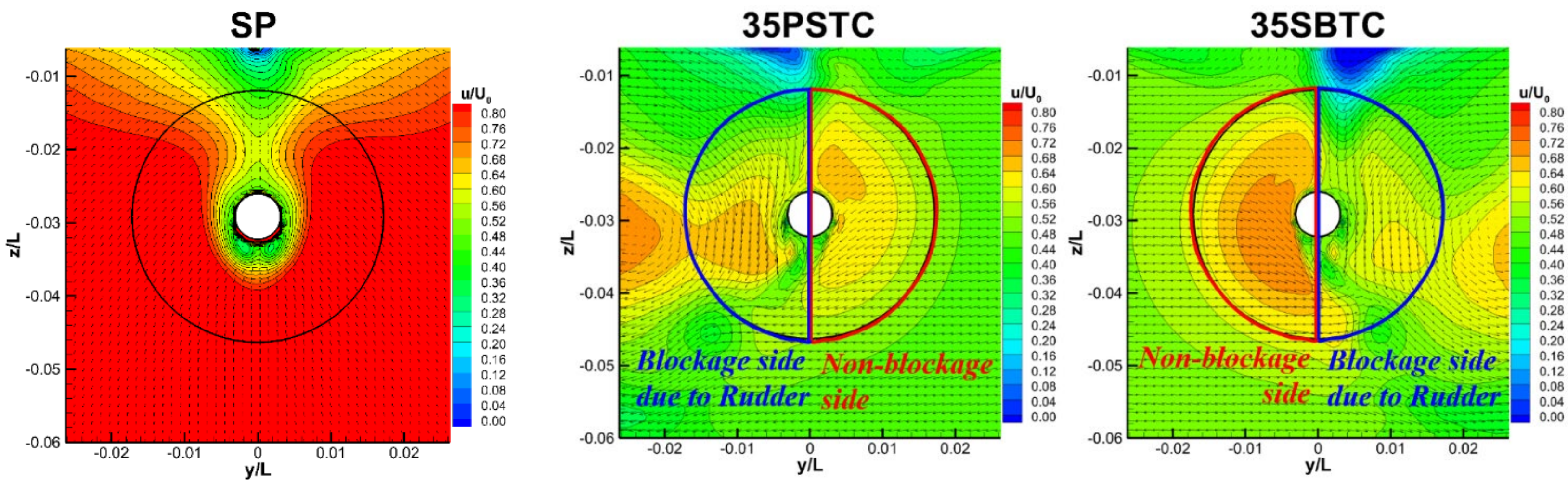

Wake coefficient of SP and TC (Fr= 0.26)

	SP	35PSTC		35SBTC	
EFD (Thrust identity method)	0.701	0.806		0.659	
CFD	0.790	0.570		0.585	
		Blockage side	**Non-blockage side**	**Blockage side**	**Non-blockage side**
		0.558	0.582	0.531	0.639

- Propeller inflow different SP due to drift-angle induced hull vortices and rudder blockage with similar trends both port and starboard, but larger magnitudes for port
- Towed CFD using free running time histories, but without propeller and both with and without rudder needed to fully explain hull-propeller-rudder interaction
- Thrust identity method significantly underestimates and overestimates the wake fraction compared CFD for SP and TC, respectively

Appendix

- Propeller more heavily loaded for turning compared SP, especially port turning
- Loss in propeller efficiency as per t' correlation induces speed loss etc. as per multiple facility standard deviation SD analysis maneuvering parameter study with larger differences for port turning

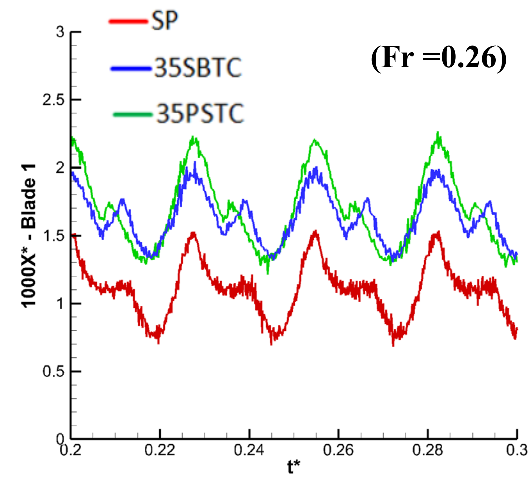

Hydrodynamic non dimensional X force of a single blade during SP, 35PSTC and 35SBTC in steady state part (phase is matched with SP and Turning) Left: Fr 0.26, Right: Fr 0.157

- KP505 propeller uses NACA66. When the Re ≅10^6,
  Max Cl/Cd of NACA66 can be achieved when AoA is ***3.25 deg***.
- Average AoA (Fr = 0.26):

SP: 4.54deg; 35PSTC: 8.52deg; and 35SBTC: 7.86deg

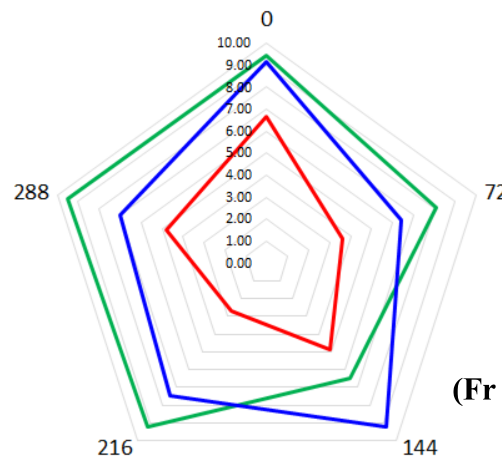

Propeller Blade Angle of attack comparison at 70% radius. Left: Fr 0.26, Right : Fr 0.157

Appendix

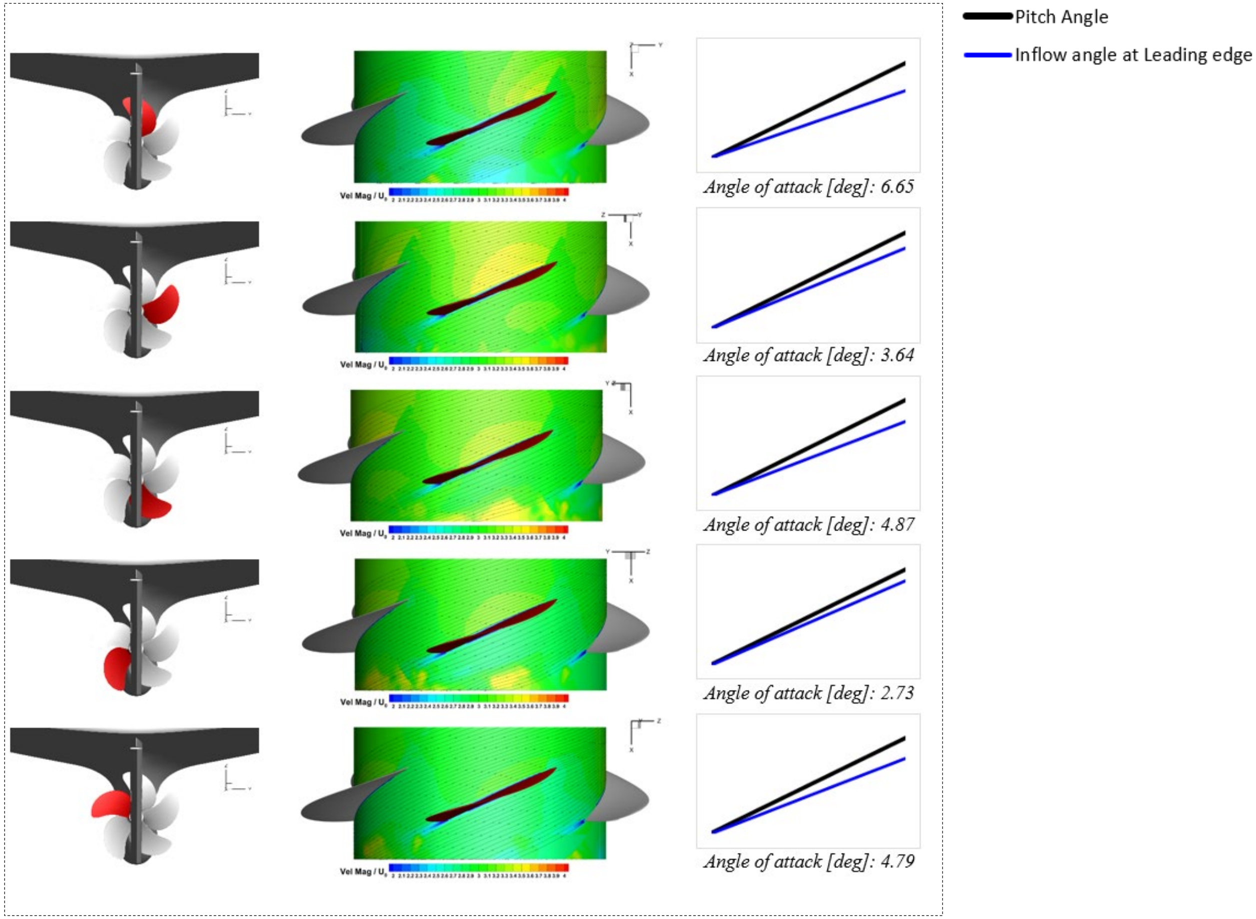

(Fr =0.26)

Propeller Blade Angle of attack at 70% radius of SP (Fr# : 0.26)

Appendix

Pitch Angle
Inflow angle at Leading edge

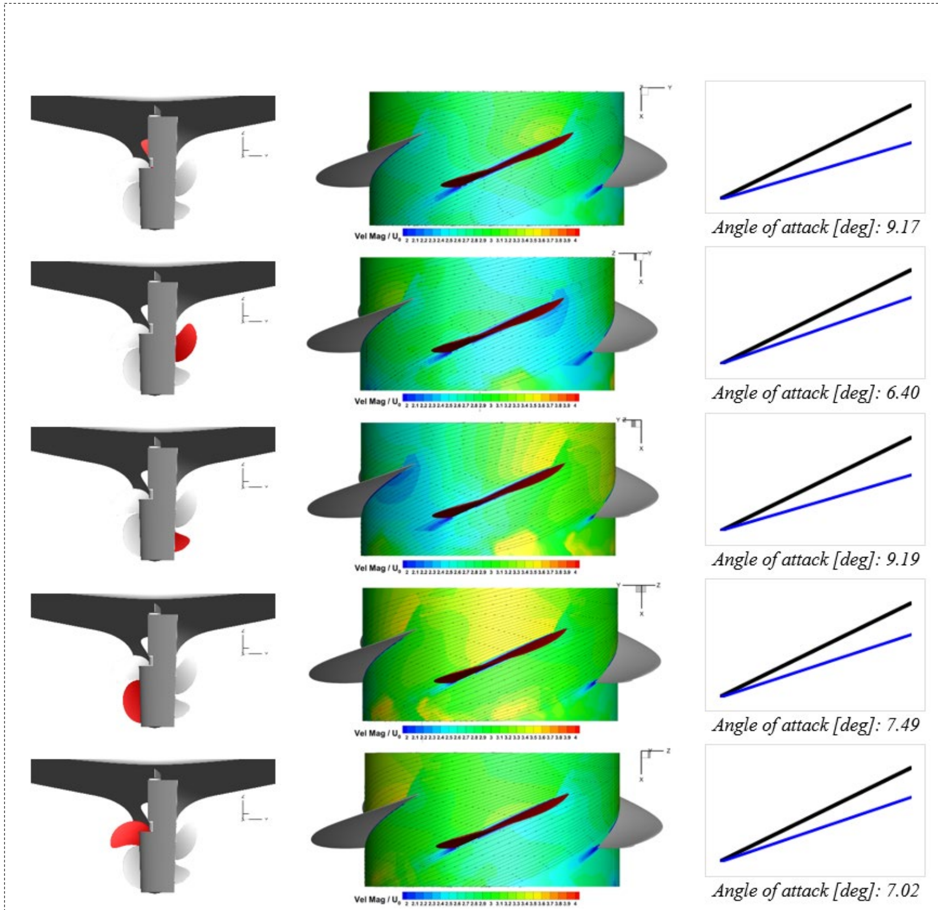

Propeller Blade Angle of attack at 70% radius of 35SBTC (Fr#: 0.26)

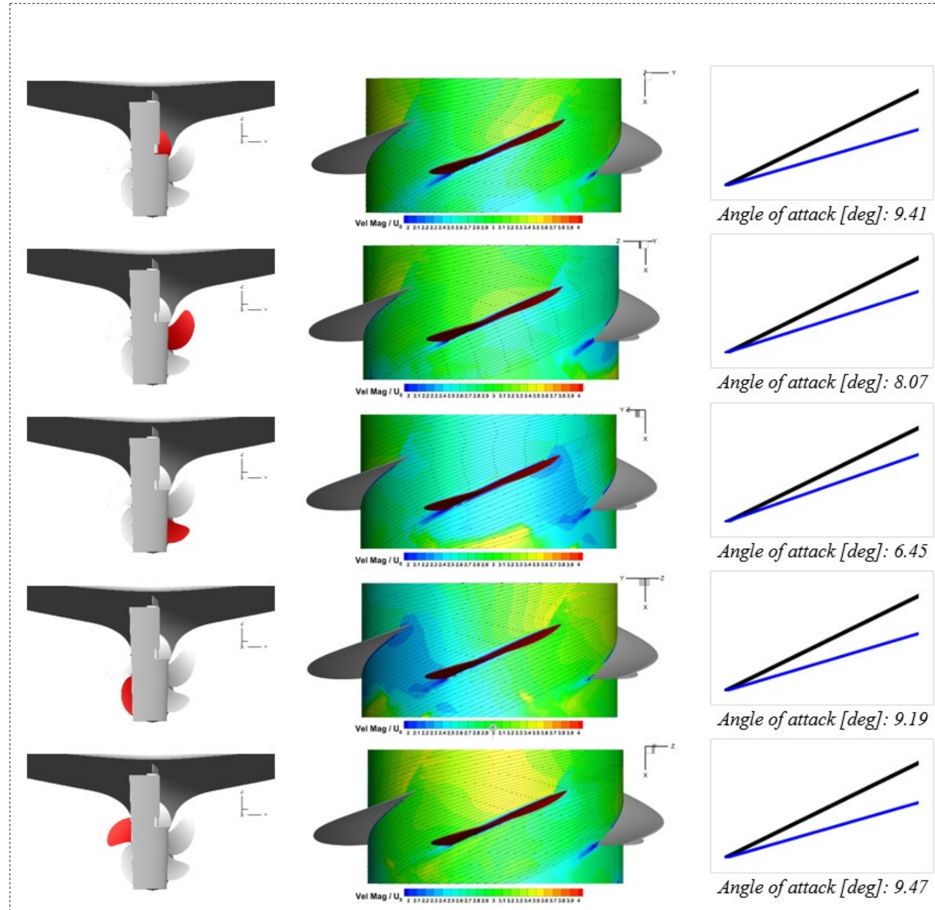

Propeller Blade Angle of attack at 70% radius of 35PSTC (Fr#: 0.26)